Consolidation and strength evolution of Caland-Beer Channel mud

Measurement report on laboratory experiments

L.M. Merckelbach

report no. 7-98

1998

The work reported herein has been financially supported by the Netherlands Technology Foundation (STW) and the Commission of the European Communities, DG XII, MAST3-COSINUS Project (Contract No. MAS3-CT97-0082).

Hydromechanics Section, Faculty of Civil Engineering and Geosciences, Delft University of Technology, P.O. Box 5048, 2600 GA, the Netherlands. Tel. +31 15 278 40 70; Fax +31 15 278 59 75; E-mail: l.merckelbach@ct.tudelft.nl

Abstract

Many harbours in the world suffer from high siltation rates in their basins. To guarantee safe shipping, harbour authorities have to maintain the navigable depth by having dredged large amounts of mud. Some authorities relate the navigable depth to a depth at which the density is equal to a certain value, e.g. 1200 kg/m^3. However, the shear strength might be a more direct criterion to relate the navigable depth to.

A research project is conducted to develop a model to describe the consolidation behaviour and strength evolution of mud layers. The second series of experiments for this project, executed at Delft University of Technology, are described in this report. The analysis of the data is left for future work.

The sedimentation and consolidation of Caland-Beer Channel mud was simulated in segmented consolidation columns. The use of segments made it possible to obtain well-defined and undisturbed samples of the mud bed. For this reason, more accurate shear vane measurements of the samples could be done than if conventional consolidation columns had been used.

Four segmented consolidation columns and one conventional consolidation column were set up. To study the time evolution of the strength of the mud bed, the segmented columns were dismantled at different times. After the dismantling, shear vane tests could be carried out and density measurements could be done with a conductivity probe. The density profiles of the mud layer in the conventional column were measured with a γ-ray densimeter. Pore water pressures were measured at several times. From these measurements effective stresses and permeabilities were calculated. Various rheological parameters were derived from four different types of shear vane measurements. Flow curves were also measured.

It turned out that the effective stresses could be approximated by a power law. Furthermore, the rheological parameters turned out to be approximately linearly interrelated, even though the parameters were derived from different types of rheological experiments. Small modifications of the experimental set-up are recommended for future experiments.

Contents

1 Introduction **3**

2 Experiments **4**
2.1 Segmented consolidation columns 4
2.2 Mud preparation 7
2.3 Measurement techniques 7
2.3.1 Density measurement 7
2.3.2 Pore water pressure measurement 10
2.3.3 Rheometric measurements 11

3 Results **16**
3.1 Mud-water interface settlement 16
3.2 Density profiles 16
3.3 Excess pore water pressure profiles 17
3.4 Effective stress data 17
3.5 Permeability data 17
3.6 Shear stress data 17

4 Concluding remarks **19**

5 Acknowledgement **22**

References **23**

List of Symbols **24**

A Figures **26**

Chapter 1

Introduction

Many harbours in the world suffer from high siltation rates in their basins. To guarantee safe shipping, harbour authorities have to maintain the navigable depth by dredging large amounts of mud, which involves substantial costs.

Typical for these basins is that a bottom is hard to define since the density increases gradually from the water surface to deep in the bed. Some authorities relate the navigable depth to the depth at which the density of the mud is equal to a certain value, e.g. 1200 kg/m^3. However, the (shear) strength seems to be a more relevant parameter for defining the navigable depth. Although density and shear strength of mud are interrelated, this relationship is not unique and may be time dependent. Both parameters are related to the consolidation behaviour. A definition of the navigable depth based on shear strength might give rise to a change in the dredging strategy and possibly result in lower costs.

Presently, a research project, which is financed by The Netherlands Technology Foundation, is conducted to develop a mathematical model of strength evolution in a mud bed. This model can be used to translate results from laboratory experiments to field conditions. The model formulation requires knowledge of consolidation and strength evolution processes. In this respect, important parameters are effective stress, permeability and (peak) shear stress. These parameters can be calculated from measurable quantities as bulk density, pore water pressure and torques exerted onto a vane introduced into a mud sample. During the period from April 28$^{\text{th}}$ until July 19$^{\text{th}}$ 1997, a first series of experiments was carried out at the University of Oxford and reported in Merckelbach (1998).

A second series of experiments was carried out at the Hydromechanics Laboratory of Delft University of Technology, Department of Civil Engineering and Geosciences during the period from April 14$^{\text{th}}$ until July 17$^{\text{th}}$ 1998. The results are reported herein. However, the analysis of the data will be left for future work. It is noted that the data reported herein are also available on CD-ROM.

This report is organized as follows. In Chapter 2 the experimental programme is discussed, including the design of the new type of consolidation columns and the measurement techniques used. In Chapter 3 the results are presented. Concluding remarks are stated in Chapter 4.

Chapter 2

Experiments

The aim of the laboratory experiments described is to simulate the formation of a mud layer formed by deposition from a suspension and to study the self-weight consolidation behaviour and strength development of this mud layer. In these experiments we made use of consolidation columns. The dimensions of the columns were determined according to the following requirements:

- The initial mud-water mixture should be a suspension. This means that the initial, uniformly distributed density should be lower than the density that corresponds to the gel point, which is approximately 1100 kg/m^3.
- The minimum bed height when consolidation is almost completed, should be about 0.5 m to make possible the measurement of a strength profile using a shear vane tester.
- The primary consolidation process should be more or less completed by the end of the measuring period.
- Side wall effects should be negligible.

From these requirements it follows that the target value of the initial density is within the range 1060–1080 kg/m^3 and, if we assume that the averaged density of the consolidated bed is about 1200 kg/m^3, the required initial height of the suspension is about 1.5 m, which is the height selected. In this situation a measuring period of at least three months is considered sufficiently long. The inner diameter selected is 100 mm, which is comparable with the diameter used in the Oxford experiments (Merckelbach, 1998). The inner diameter chosen is expected not to result in adverse wall effects, see (Bowden, 1988; Berlamont *et al.*, 1992; Berlamont & van Goethem, 1984).

2.1 Segmented consolidation columns

A key measurement in the experiments was the shear vane test for which we used a sensitive rheometer equipped with a vane. If used in conventional consolidation columns we would need a vane with a very long shaft or with an extensible shaft to be able to measure shear strengths deep in the bed. This would lead to a significant contribution to the torque measured caused by friction along the shaft. Moreover, centering of a vane with a long shaft was expected to be troublesome. Manually extending the shaft would lead to significant adverse effects on the

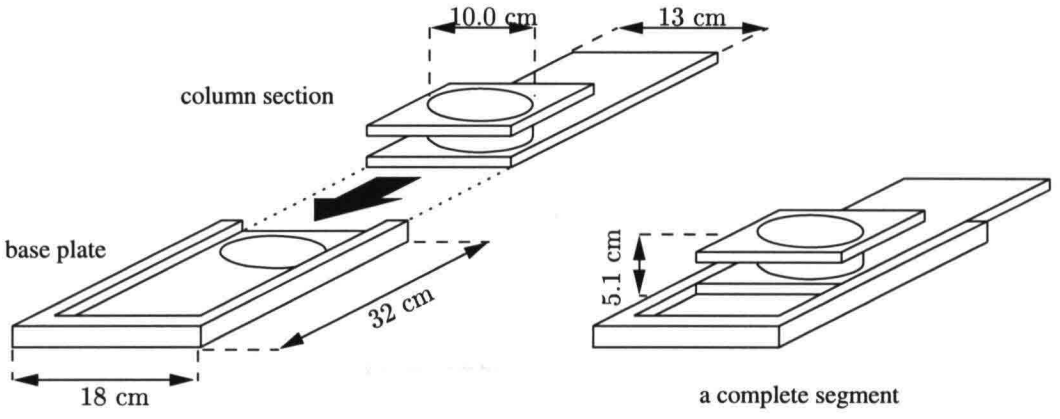

Figure 2.1: A base plate, a column section and a complete segment

measurements, as was experienced during the first series of experiments (Merckelbach, 1998). To avoid these problems and to make use of the capabilities of the rheometer, we designed a new type of consolidation columns.

The basic idea was to divide the consolidation column into two sections: a lower section where the shear vane tests would take place, and an upper section to provide the necessary (initial) height. The height of the lower section was chosen such that the consolidation of the mud layer was expected to be completed within the lower section at the time shear vane tests would be carried out.

The procedure was as follows. Prior to the shear vane tests, the overlying water was let out of the column. Then, the upper section was removed, leaving the lower section with the mud bed. The lower section itself was also divided into multiple sections, called segments. Each segment was a combination of a column section and a base plate, see Figure 2.1. The overall height of a segment, including an O-ring used for sealing the segments, was 5.1 cm. The segments were designed such that well-defined samples could be isolated from the column. This was done by pushing the column section onto the base plate, and then taking the whole segment away by carefully sliding it aside. Manipulating each segment in the column in this way, starting with the uppermost segment, the column was sliced into well-defined and equally shaped samples. These samples were used for taking shear strength measurements and density measurements. The dismantling procedure is visualized in Figure 2.2.

As the shear vane test destroys the structure of the material significantly, we needed multiple, equally set up columns to study the strength evolution with time. To cover the time span of three months, shear vane tests were initially scheduled at $1\frac{1}{2}$, 3, 6 and 12 weeks[1]. Consequently, four columns were needed. A total number of 38 segments were available to build the lower sections of the four columns. The set-up that we used is shown in Table 2.1. The columns are labeled "TDxx" where xx is a number indicating the duration in days of the particular experiment.

In addition to the four segmented columns, a conventional column was set up. This column was equipped with a γ-ray densimeter, provided by the Dutch dredging company H.A.M. By using the γ-ray densimeter, density profiles were obtained without affecting the structure of the mud. In this way, the density development with time was monitored. Consecutive density

[1]The actual measurements were made on days 9, 24, 58 and 95.

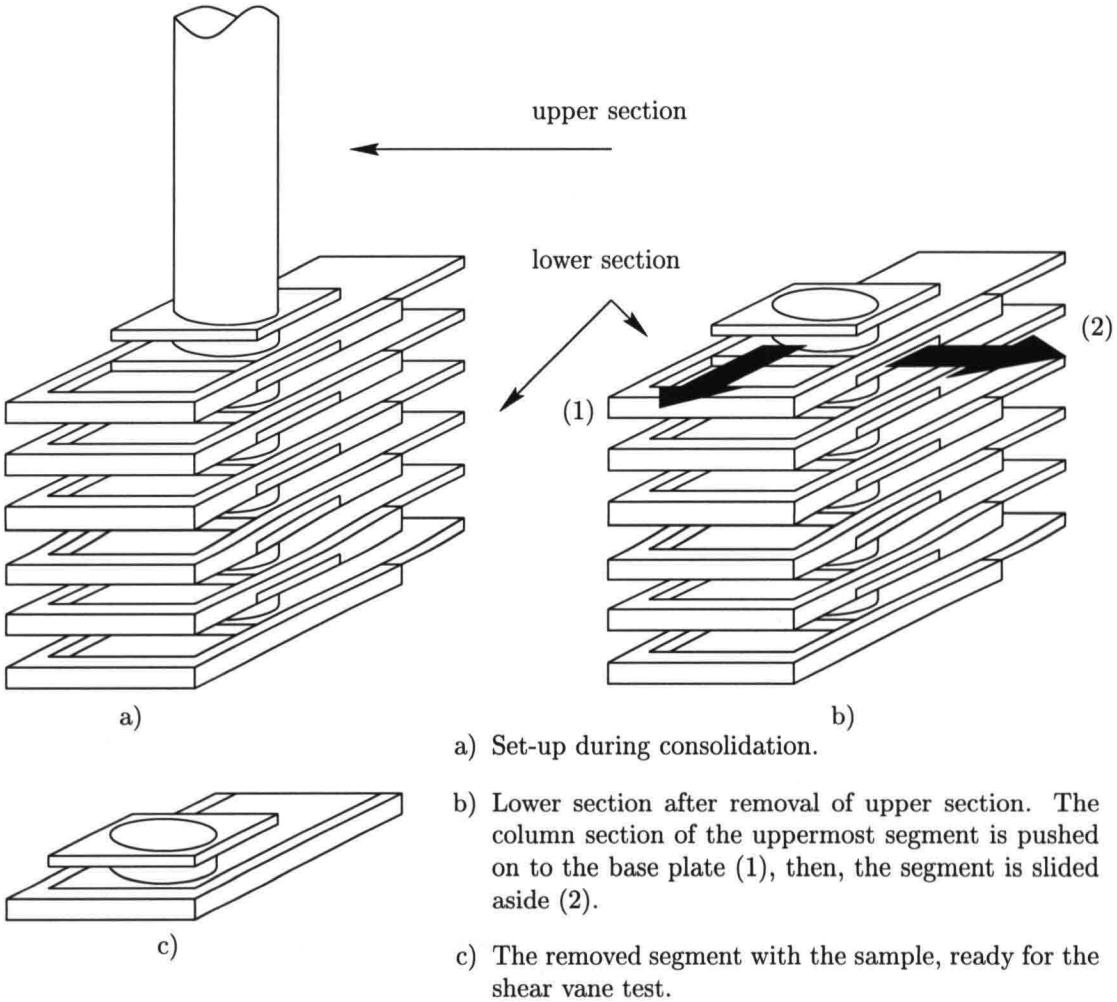

a) Set-up during consolidation.

b) Lower section after removal of upper section. The column section of the uppermost segment is pushed on to the base plate (1), then, the segment is slided aside (2).

c) The removed segment with the sample, ready for the shear vane test.

Figure 2.2: A schematic picture of the dismantling of a segmented column

Table 2.1: Column layout

	Number of segments	Height of lower section (m)
TD9	12	0.60
TD24	10	0.50
TD58	8	0.40
TD95	8	0.40

profiles were used to estimate the permeability. Because of the length of the column, no vane tests could be carried out. Instead, at the end of the experiment (TD95) two mud samples were taken and used for flow curve measurements. The conventional column is labelled "TDC".

2.2 Mud preparation

The mud that was tested was Caland-Beer Channel mud (Port of Rotterdam, The Netherlands). It was dredged on April 7th 1997. Its bulk density[2] was about 1.25×10^3 kg/m^3. A few properties of the Caland-Beer Channel mud are listed in Table 2.2. A particle size distribution is presented in Figure 2.3

Table 2.2: Properties of Caland-Beer Channel mud

density of solids ($\times10^3$ kg/m^3)	2.5278 $\pm$0.006
sodium adsorption ratio (-)	70
cation exchange capacity (cmol/kg)	20.1
specific surface (m^2/g)	96
humus (% by weight)	3.99

The mud used in the experiments was diluted to a density of 1.080×10^3 kg/m^3. The diluent was sea water, taken at the beach at Hook of Holland. Before the mud suspension was introduced into the columns, it had been mixed thoroughly for one hour.

An overview of the initial conditions is presented in Table 2.3.

2.3 Measurement techniques

2.3.1 Density measurement

One of the basic parameters measured in the present experiments is density. The measurement technique used, depended on the type of column involved. The bulk density of the mud in the segmented columns was measured by using a conductivity probe, whereas the bulk density of the mud in the conventional column was measured by using a γ-ray densimeter.

[2]The density of the slurry as it was supplied by the dredging company. This density is generally not equal to the in-situ density.

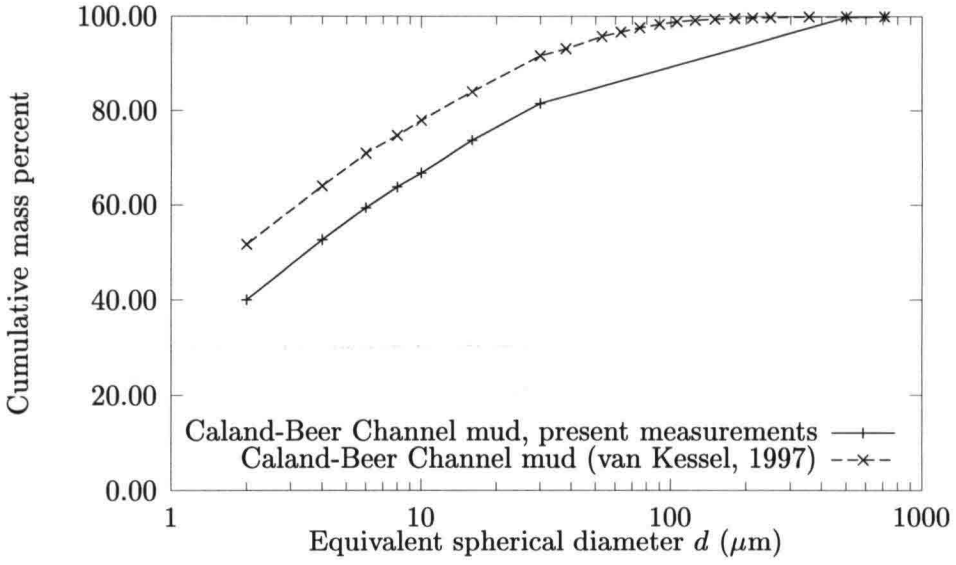

Figure 2.3: Particle size distribution

Table 2.3: Properties of the mud suspensions introduced

	Pore water density (kg/m^3)	Initial bulk density (kg/m^3)	Initial height (m)
TD9	1013	1080	1.538
TD24	1013	1080	1.537
TD58	1013	1080	1.546
TD95	1013	1080	1.536
TDC	1013	1080	1.546

The measuring principle of the γ-ray densimeter is that the absorption of γ-rays by matter can be related to the mass of that matter. Besides the mud within the column, the column wall will also absorb radiation. The effect of absorption of radiation by the column wall is easily accounted for by the calibration constants provided the column is prismatic. Unfortunately, columns consisting of segments were not prismatic and thus measuring the density using a γ-ray densimeter would be quite complex. Therefore, the γ-ray densimeter was applied to the conventional column only.

Segmented columns: conductivity probe

Measurement principle

The principle of the conductivity probe, which was supplied by Delft Hydraulic, is as follows, see also (De Wit, 1995). An electrical current can be established between two submerged electrodes, because of the presence of free moving ions in water. Keeping the magnitude of the current I at a constant value and measuring the voltage between the electrodes V, the

resistance R can be calculated from Ohm's law

$$R = \frac{V}{I}. \tag{2.1}$$

The resistance R depends on the resistivity r, the distance between the electrodes l and the cross sectional area A according to (Weast, 1973)

$$R = r\frac{l}{A}. \tag{2.2}$$

The water is conductive because of the presence of ions, whereas the sediment is assumed to be non-conducting. An increase in the volume fraction sediment reduces the amount of ions per unit volume, so that the resistivity increases as well. Thus, the voltage difference is proportional to the resistivity, which follows from (2.1) and (2.2). The resistivity is proportional to the reciprocal of the volume fraction of water, which leads to

$$c = k_1 + k_2\frac{1}{V}, \tag{2.3}$$

where c is the concentration. The constants k_1 and k_2 can be determined by measuring the voltage difference of clear water V_0 and measuring the voltage difference V_s of a sample with a known concentration c_s. This results in the following relationship between the concentration and the voltage difference:

$$c(V) = c_s\left(\frac{V_s}{V_s - V_0}\right)\left(\frac{V - V_0}{V}\right). \tag{2.4}$$

The bulk density is determined by

$$\rho_b(c) = \rho_f + c\left(1 - \frac{\rho_f}{\rho_s}\right). \tag{2.5}$$

Usage

Density profiles were obtained by lowering the conductivity probe in the bed. However, the conductivity probe affects the structure of the mud and, as a consequence, lowering the probe into the bed would certainly have an adverse effect on the results of the vane tests. Therefore, the density measurements were done after the vane tests. This implies that the overall density profile is a compilation of the profiles of the individual segments. It is noted that measurements closely near the surface and the bottom of the sample usually result in too high values for the density. This is because the interfaces at the surface and the bottom decrease the electrical conductivity. These artificial density anomalies were filtered out by a data post-processing procedure. The accuracy of the density measurement is estimated at $\pm$ 15 kg/m^3.

Conventional column: γ-ray densimeter

The γ-ray densimeter used, was a LB370 densimeter, manufactured by Berthold GmbH. The measurement principle of the γ-ray densimeter, is based on the absorption of γ-rays by matter, similar to the absorption of X-rays, see Been (1980).

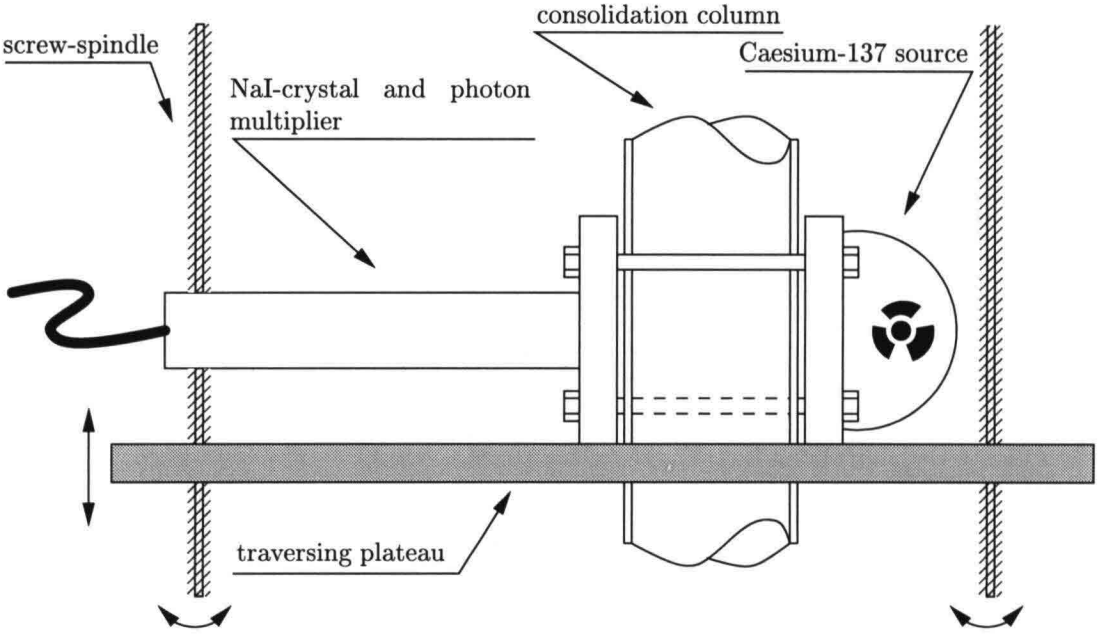

Figure 2.4: A schematic representation of the γ-ray densimeter

The source of the LB370 is Caesium-137, a radioactive material that emits mainly photons of high energy, so called γ-rays. The source is shielded by a lead housing. Locally the shield can be opened to produce a narrow bundle of γ-rays. The γ-rays are passed through the consolidation column and detected at the other side by a NaI-crystal that converts gamma-photons to light-photons. The signal is enhanced by a photon multiplier tube. Subsequently, the light pulses are converted into an electric current. The electric current is manipulated by an electronic unit that eventually produces an output in Volts. A sketch of the γ-ray densimeter is shown in Figure 2.4. The bulk density is related to the voltage by the relation

$$\rho_b = AV + B, \tag{2.6}$$

where ρ_b is the bulk density, V the output of the γ-ray densimeter and A and B are calibration constants. It is noted that the usual exponential relationship between density and the count rate of light pulses (Been, 1980) is dealt with within the electronic unit.

The accuracy of the density measurements is $\pm$ 3 kg/m^3. The vertical resolution, determined by the diameter of the γ-ray bundle, is about 2 cm.

2.3.2 Pore water pressure measurement

The method used to measure pore water pressures is largely based on the method commonly used in the Soil Mechanics Laboratory of the University of Oxford, see Merckelbach (1998). At different heights pore water pressures ports were let into the column wall. Each port was provided with a *vyon* plastic filter. The ports were connected to a pressure measuring unit via tubes. The pressure measuring unit housed one pressure transducer (PDCR 810) that could be connected to any of the pressure ports, one at a time. The pressure measuring unit has been modified with respect to the unit used in Oxford, but in design only. The rotating disk

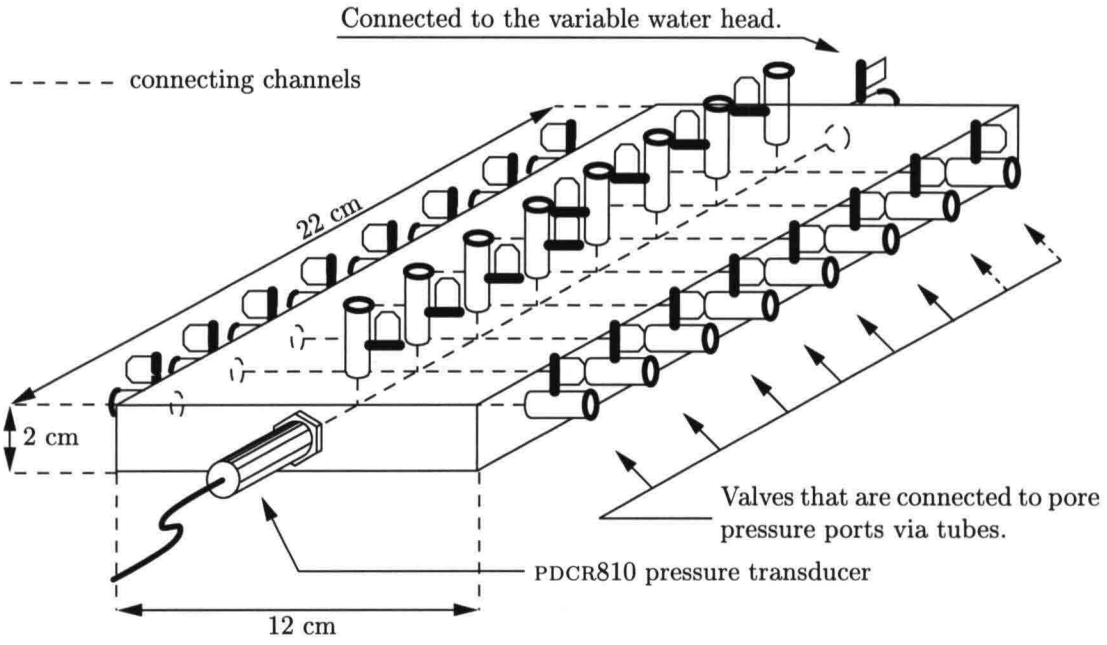

Figure 2.5: Pressure measuring unit

principle to connect the transducer to one of the pressure ports has been replaced by the use of valves, see also Figure 2.5.

The transducer was calibrated by connecting it to a variable water head, ranging 1.0 m in height. The calibration procedure was carried out prior to the actual measurements. The accuracy of the pore water pressure readings is 1 mm water head or 10 Pa.

2.3.3 Rheometric measurements

The strength measurements were done by using a UDS 200 rheometer, manufactured by Physica GmbH. The standard measuring device is a concentric-cylinder geometry. The main disadvantage of this, and similar devices is that the material has to be injected in a container before testing. This implies that the structure of the sample has changed before testing. To avoid structural changes by the measuring method as much as possible we chose to use a vane instead. The advantages of a vane are that the structural changes by inserting the vane are minimal and the material is sheared within itself, because there are no side walls. A disadvantage is that the flow pattern is less well defined.

Shear vane test

The major part of the rheometric measurements were carried out with a vane. The dimensions of the vane used were 2.0 cm in height and 1.0 cm in diameter. The vane consisted of five equally angled, rectangular blades, as shown in Figure 2.6.

The three basic parameters recorded by the rheometer were time, rotation angle of the device (vane) and the torque exerted on the device. The conversion from torque to shear stress requires two assumptions. Firstly, it is assumed that the surface of maximum shear is cylindrically shaped. Especially in the vicinity of the tips of the vane blades this may be

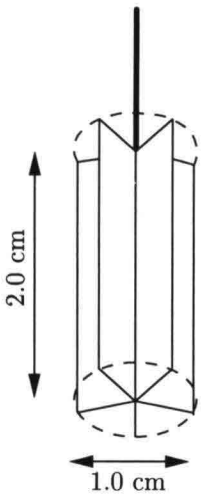

Figure 2.6: Five-bladed vane

questionable, but it is a generally accepted assumption. Secondly, it is assumed that the stress distribution along the assumed shear surface is uniform over the height. Neglecting the friction along the shaft, the conversion from torque to shear stress is given by

$$\tau = \frac{T}{2\pi l r^2 \left(1 + \frac{2r}{3l}\right)}, \tag{2.7}$$

where τ is the (averaged) shear stress, T is the recorded torque, l is the height of the vane and r is the radius of the vane.

Basically, three different types of measurements were carried out, namely rate controlled measurements, stress controlled measurements and oscillating, rate controlled measurements.

Rate controlled measurements

In the rate controlled measurements the vane was rotated with a preset and constant angular velocity. The torque exerted on the vane was recorded. Two different angular velocities were used: 1.0 rpm and 0.1 rpm.

A typical recording is shown in Figure 2.7. (The inset in this figure shows the initial part of the curve.) This figure shows that the stress quickly increases with increasing rotation angle, until a certain maximum is reached after which it gradually decreases to a certain constant stress. The curves are parameterized by defining four parameters. The first characteristic parameter is the peak shear stress, τ_{peak}, and is defined as the highest recorded value. The second parameter is the peak angle, ϕ_{peak}, which is the rotation angle that pertains to the peak shear stress. The third parameter is the residual shear stress, τ_{residual}, which is defined as the shear stress after 2 complete revolutions. The residual shear stress is calculated by the averaging the shear stress over $\phi \in [690°, 720°]$, i.e. the last 30 degrees. However, the measurements at a rotation speed of an angular velocity of 0.1 rpm only covered the first 35 degrees, so that for those tests the residual shear stresses could not be determined. The fourth parameter is the tangent to the curve in the origin, $\frac{\mathrm{d}\tau}{\mathrm{d}\phi}$. The tangent cannot be calculated directly from the curve, but it is estimated by extrapolation. It is assumed that for small

angles the material behaves according to a viscoelastic Maxwell body. Then the curve of shear stress against rotation angle can be approximated by an expression of the form of $\tau = A[1 - \exp(-B\phi)]$, where A and B are coefficients. These coefficients are determined by fitting the formula through the first two data points. Accordingly, $\frac{d\tau}{d\phi}$ is given by

$$\left.\frac{d\tau}{d\phi}\right|_{\phi=0} = AB \tag{2.8}$$

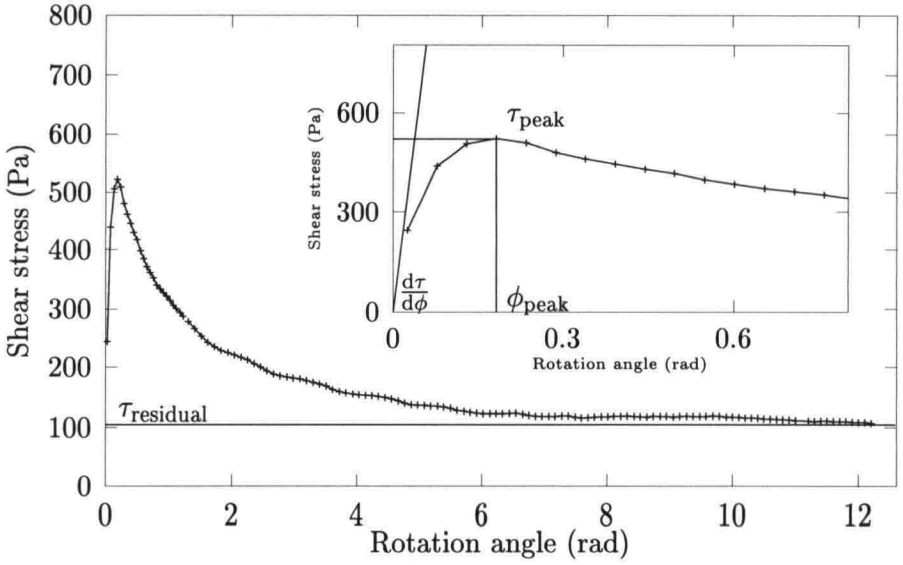

Figure 2.7: A typical recording of a rate controlled measurement.

Stress controlled measurements

In the stress controlled measurements the stress (actually a torque) was prescribed and the resulting rotation angle was recorded. During a time interval of 300 seconds, the shear stress was increased logarithmically starting from $\tau \approx 3$ Pa until $\tau \approx 3000$ Pa ($T = 0.01$ mNm until $T = 10$ mNm). However, each measurement was aborted shortly after the material started to flow. A typical curve is shown in Figure 2.8. This curve is characterized by a yield stress, τ_{yield}, at which the material is said to start to flow. From inspecting the data files it followed that there exists a clear jump in angular velocities from values of the order of 0.001 rad/s to the order of 1.0 rad/s within three data points. Accordingly, the on-set of motion is defined as the point when the angular velocity equals 0.01 rad/s. Both the yield stress and rotation angle at the yield point, ϕ_{yield}, are determined by linear interpolation.

Oscillating, rate controlled measurements

Both the rate controlled and the stress controlled measurements result in deformations that are so large that the structure of the material around the vane changes significantly. An oscillating rate controlled measurement for very small amplitudes provides a method to determine

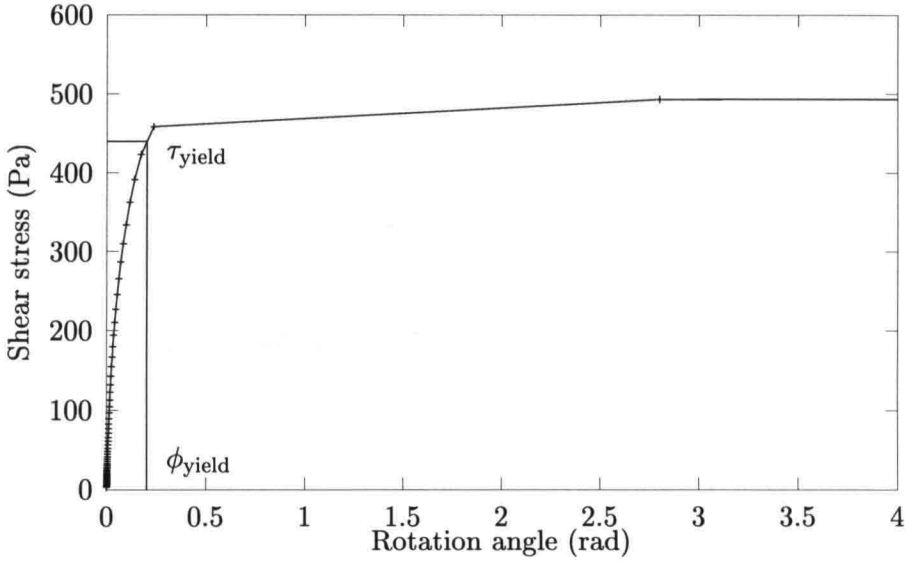

Figure 2.8: A typical recording of a stress controlled measurement.

the storage modulus and loss modulus within the linear range, that is, the range in which the structure remains in tact.

During an oscillating, rate controlled measurement the rotation angle of the vane is prescribed by the function

$$\phi(t) = \hat{\phi}\sin(\omega t), \tag{2.9}$$

where $\hat{\phi}$ is the amplitude of the rotation angle, ω is the angular frequency and t is time. For small deformations the response can be considered linear, which means that the recorded shear stress is also sinusoidal:

$$\tau(t) = \hat{\tau}\sin(\omega t + \delta), \tag{2.10}$$

where $\hat{\tau}$ is the shear stress amplitude and δ is a phase shift, called the loss angle. The shear stress can also be written as

$$\tau(t) = \hat{\phi}\left(G'\sin(\omega t) + G''\cos(\omega t)\right), \tag{2.11}$$

where G' is the storage modulus and G'' is the loss modulus. Combining (2.10) and (2.11) yields

$$\tan\delta = \frac{G'}{G''}. \tag{2.12}$$

For purely elastic materials the storage modulus equals zero ($\delta = 0$), whereas for purely viscous materials the storage modulus equals zero ($\delta = \frac{\pi}{2}$). It is noted that equations (2.9) and (2.11) are usually expressed in terms of strain rather than rotation angles of the vane. However, the relationship between rotation angle and strain is not clear. As long as the conversion from rotation angle to strain has not been done, the values of G' and G'' cannot be compared with the moduli obtained from other rheometric experiments, e.g. experiments that use a small-gap concentric-cylinder measuring device, which do have a well-defined relationship between rotation angle and strain.

Oscillating experiments were carried out for several angular frequencies. Typical results are shown in Figure 2.9. The figure shows that both the storage modulus and the loss modulus are weakly dependent on the angular frequency, approximately according to a power law. The storage modulus and the loss modulus corresponding to an angular frequency of 1.57 rad/s are used as characteristic values.

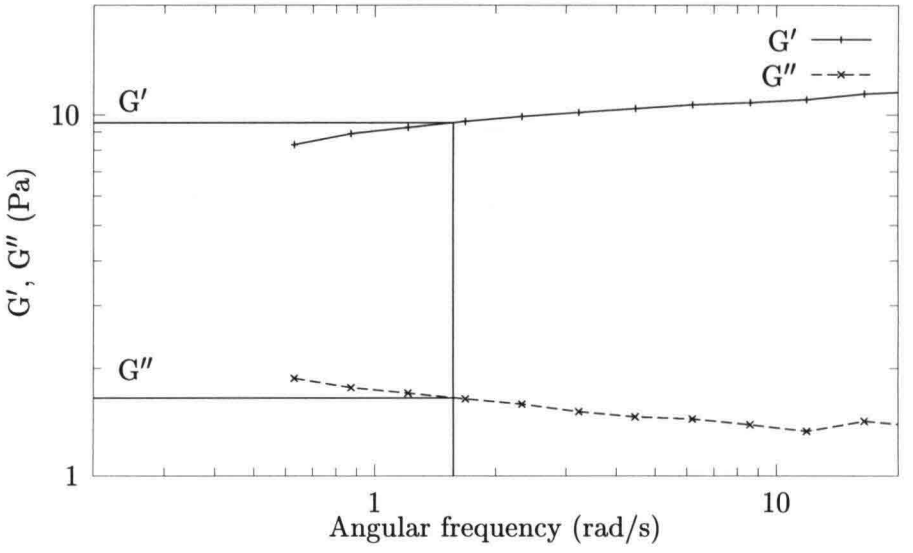

Figure 2.9: A typical recording of an oscillation measurement.

Flow curve measurements

Many rheometric experiments are reported in literature. Standard rheometric devices as plate-plate, cone-plate and concentric-cylinder are very popular. The main advantage of these rheometric measurements is the relatively well known relation between the rotation of the device and the strains within the materials. Unfortunately, accurate *in-situ* tests using these techniques are nearly impossible, since introducing the mud into the container of the device causes significant deformations. However, flow curves of remoulded material can be used to compare with other flow curve measurements, not necessarily of the same type of mud. Two flow curve measurements with a concentric-cylinder device were carried out after the experiment had finished. The mud was taken from the conventional column. Before the mud was introduced into the container, it was mixed thoroughly. The averaged density of both samples was 1210 ± 10 kg/m^3.

Chapter 3

Results

3.1 Mud-water interface settlement

The level of the mud-water interface was measured at different times during the experiments. The measurements are shown in Figure A.1. The interface dropped from 1.53 m (initial height) to about 0.90 m within one day. Subsequently, the settling velocity gradually decreased. Significant deformations did not occur anymore after about 50 days. The correspondence between the interface heights of the different columns is fair.

3.2 Density profiles

In contrast with the conventional column, in which several density profiles were measured, only one density profile was measured of each segmented column. In Figures A.2 through A.5 the density profiles of the four segmented columns (TD9, TD24, TD58 and TD95) are shown together with the corresponding density profile of the conventional column.

The agreement between the measurements of the segmented columns on one hand, and the conventional column on the other, is fair. The measurements done with the conductivity probe show some scatter, but the data points are mostly within the range of accuracy.

An exception, however, is the density profile of TD24 (Figure A.3), of which the density data points below 0.3 m do not seem realistic.

For the permeability calculations it is required to have density profiles that cover the whole mud bed. Unfortunately, in the present set-up the γ-ray densimeter could not reach the positions required to measure the density of the lowermost 12 cm of the mud bed. For the sake of the permeability calculations the density at bottom was estimated by taking into account that the integrated mass should be constant with time. The estimated density points correspond reasonably well to the densities at the bottom measured with the conductivity probe, except for experiment TD24.

In Figure A.6 the available density profiles measured in the conventional column are collected. This figure shows the development of the density distribution of the conventional column (TDC) with time.

3.3 Excess pore water pressure profiles

The excess pore water pressure profiles are shown in Figures A.7 through A.11. The results of the pore water pressure measurements of the segmented columns do not show any anomalies. However, in the conventional column excess pore water pressures greater than zero were calculated just above the mud-water interface on day 15, 34, 58 and 95. This was probably caused by the presence of a water layer with increased salinity. The density measurements made on day 15 and day 58 support this explanation, see Figure A.6.

3.4 Effective stress data

Generally, the effective stress is defined as the total stress minus the pore water pressure. Total stresses are easily obtained by integration of the density profiles. The effective stress data are shown in Figures A.12 through A.16.

The effective stress data are presented in two different ways. The first way is effective stress (σ') against volume fraction of solids (ϕ_p). This plot uses the lower axis (volume fraction) and the left-hand axis (effective stress). The symbol used for the data points is '+'. Notice that both axes are on logarithmic scales.

The second way is effective stress against void ratio (e). This plot uses the upper axis (effective stress) and the right-hand axis (void ratio). The symbol used for the data points is '•'. These axes are on linear scales.

The accuracy of the effective stress data, which depends on the accuracy of both the pore water pressure measurement and the density measurements, is estimated at ±15 Pa.

3.5 Permeability data

Permeability was calculated from Darcy's law:

$$k = -\frac{1}{v_s}\frac{\partial p_e}{\partial z}, \tag{3.1}$$

where v_s is the settling velocity of the solids, k is the permeability and $\frac{\partial p_e}{\partial z}$ the excess pressure gradient. The settling velocity is calculated from two consecutive density profiles. The excess pressure gradient used in (3.1) is the average of the excess pressure gradients pertaining to these two density profiles. The calculation procedure is described in more detail by Merckelbach (1998).

Since the calculation of permeability requires at least two density profiles, the permeability data are available for the conventional column (TDC) only. The permeability data are presented in Figure A.17. The time indicated for each series of measurements is the average of the times of the two density profiles used in the calculation. The accuracy is estimated at $\pm 1.0 \times 10^{-6}$ m/s.

3.6 Shear stress data

Rate controlled shear vane tests

The peak shear stresses (τ_{peak}) and the peak angles (ϕ_{peak}), measured with the rate controlled shear vane test at Ω=1.0 rpm and Ω=0.1 rpm, are shown in Figures A.18 through A.21. The

segments are numbered starting from the interface and ending at the bottom. Note that each segment has a height of 5.1 cm.

The peak shear stresses increased with increasing depth and time, as expected. The peak shear stresses obtained at a rotation speed of $\Omega = 1.0$ rpm were generally higher than those obtained at a rotation speed of $\Omega = 0.1$ rpm. As opposed to this result, the peak angles remained more or less constant at 0.2 rad, irrespective depth and time.

The residual shear stresses (τ_{residual}) and the initial curve gradients ($\frac{\mathrm{d}\tau}{\mathrm{d}\phi}\,|_{\phi=0}$) are shown in Figures A.22 through A.25. The residual shear stresses for $\Omega 0.1$ rpm were not determined, since these tests only covered the first 35 degrees. The residual shear stresses for $\Omega = 1.0$ rpm and the initial curve gradients also increased with depth and time, as expected. The initial curve gradient for $\Omega = 0.1$ rpm is generally greater than the gradient for $\Omega = 1.0$ rpm. The initial curve gradient data points show some scatter, which was probably caused by the fitting procedure based on only two data points.

Stress controlled shear vane tests

The yield stresses (τ_{yield}) and the yield angles (ϕ_{yield}), measured with the stress controlled shear vane test, are shown in Figures A.26 through A.29. The yield stresses also increased with increasing depth and time, whereas the yield angles remained more or less constant at 0.2 rad.

Oscillating shear vane tests

The storage moduli (G') and the loss moduli (G'') at $\omega = 1.57$ rad/s are shown in Figures A.30 through A.33. Both the storage moduli and the loss moduli increased with increasing depth and time. The similarity between corresponding G'-curves and G''-curves is remarkable. The tangent of the loss angle, calculated for all data points, equals

$$\tan\delta = \frac{G''}{G'} = 0.1635 \pm 0.0094. \tag{3.2}$$

This means that the loss angle is invariant with respect to depth and time.

Flow curve measurements

The flow curves obtained with the concentric-cylinder device are shown in Figure A.34 and Figure A.35. The shear stress and differential viscosity (η) are plotted against the shear rate ($\dot{\gamma}$). The test was repeated once. The reproducibility of the flow curve measurement is satisfactory, in particular the reverse measurements ($\dot{\gamma} = 100 \rightarrow 0.01$ s^{-1}).

Chapter 4

Concluding remarks

The following concluding remarks can be made concerning the present experiments.

Segmented columns

For the present series of experiments segmented consolidation columns were designed and built. The special feature of these columns was that, after some time of consolidation, the mud layer could be sliced into well-defined samples, which, in turn, were subjected to shear vane tests.

After having dismantled four columns, we are able to evaluate the design. Setting up the columns was quite an effort; each connection between segments is a potential leakage. Since many of them were used, it was not easy to free the column from all leakages. However, when a column was leakage free, it remained so until its dismantling. The dismantling process was free of problems: even after three months, all samples could be easily pushed on to the base plate. Well-defined, undisturbed samples were obtained. All of them were suitable for testing. For similar future experiments, no modifications of the design are recommended.

Measurement techniques

We encountered minor complications with the pore water pressure measurements, density measurements with conductivity probe and density measurements with the γ-ray densimeter.

Problems with pore water pressure measurements were indicated by the calculation of small negative excess pore water pressures in the overlying water in some cases. The cause was that the density of the (fresh) water within the tubes that connected the pore pressure ports to the pressure measuring unit, slowly increased. The increment in density was the result of the diffusion process induced by the difference in salinity between the (initially fresh) water within the tubes and the salt pore water. Unfortunately, the actual density of the water within the tubes could not be measured during the experiment. Consequently, the data were corrected indirectly. It was assumed that the density within the tubes increased with time, but all tubes of a particular column with the same amount. As soon as at least two pressure ports were in the overlying water, the change in density could be estimated by requiring that the excess pore water pressures calculated for those pressure ports, were equal to zero. For similar future experiments it is recommended to adjust the salinity of the water within the tubes to the salinity of the pore water.

The problems with the conductivity probe were related to its calibration. The usual calibration procedure is to determine the calibration line by using a pore water sample and a sample of the mud bed itself. The density of both samples are determined afterwards. Apparently, the calibration line changed significantly during the measurements of TD24, resulting in an unreliable density profile. Fortunately, such a shift did probably not occur during the measurements of TD9. For the subsequent measurements (TD58 and TD95) the probe was calibrated before profiling each segment. This method is also recommended for similar future experiments.

The problems with the γ-ray densimeter were also related to the calibration procedure. Initially it was assumed that it was sufficient to calibrate the densimeter before starting the experiment considering the long half-life of Caesium-137 of about 33 years. For reasons of safety, this assumption could not be verified. Unfortunately, the assumption proved to be wrong soon after the start of the experiment, so that it was necessary to calibrate the densimeter during the experiment. However, this was not easily done since the traversing height was too limited to create enough space between the source and detector for the placing of a calibration sample. Lowering the column a few centimeters was enough to overcome this problem. For future experiments it is recommended to use strips that can be placed between the source and detector, even when the consolidation column is present. The equivalent density of each strip should be determined before the start of the experiment. Furthermore, the set-up should be modified so as to enable the measurement of the density in the lowermost 12 cm of the conventional column. Moreover, it might be worthwhile to investigate the possibility of having the traversing plateau driven by a motor in order to measure density profiles continuously.

Results

In Figure 4.1 the effective stress data are plotted against the volume fraction of solids for the experiments TD9, TD24, TD58 and TD95. The curves of TD9, TD58 and TD95 correspond quite well. Moreover, the curves appear as straight lines on double log scales, which means that the effective stress can be approximated by a power law of the volume fraction of solids. This result was also found in the first series of experiments carried out in Oxford (Merckelbach, 1998).

An exception is the curve of TD24, which is probably caused by the unreliable density measurement of TD24.

The rheological measurements showed that the parameters that can be related to strength, (τ_{peak}, τ_{residual}, τ_{yield}, G' and G''), all increased with increasing depth and time. However, this general behaviour is not only qualitative: all the parameters are more or less linearly interrelated, see Figure 4.2. Furthermore, it was observed that the rotation angle at which the peak shear stress was reached in the rate controlled measurements was practically the same as the rotation angle at the yield point in the stress controlled measurements. Moreover, these angles remained constant with respect to depth and time.

Summarizing it can be stated that the present experiments provided a data set with consistent findings. The data will be analyzed in future work.

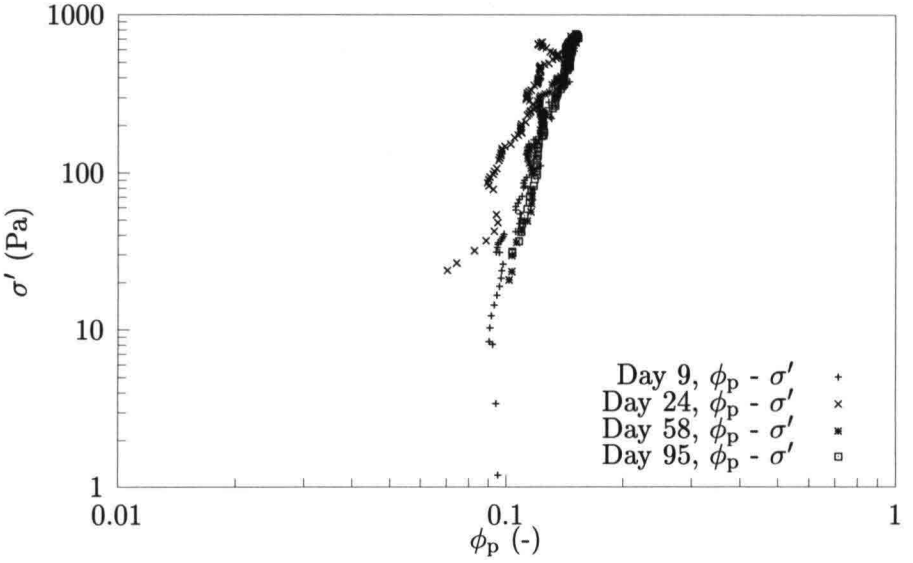

Figure 4.1: Effective stress data of TD9, TD24, TD58 and TD95

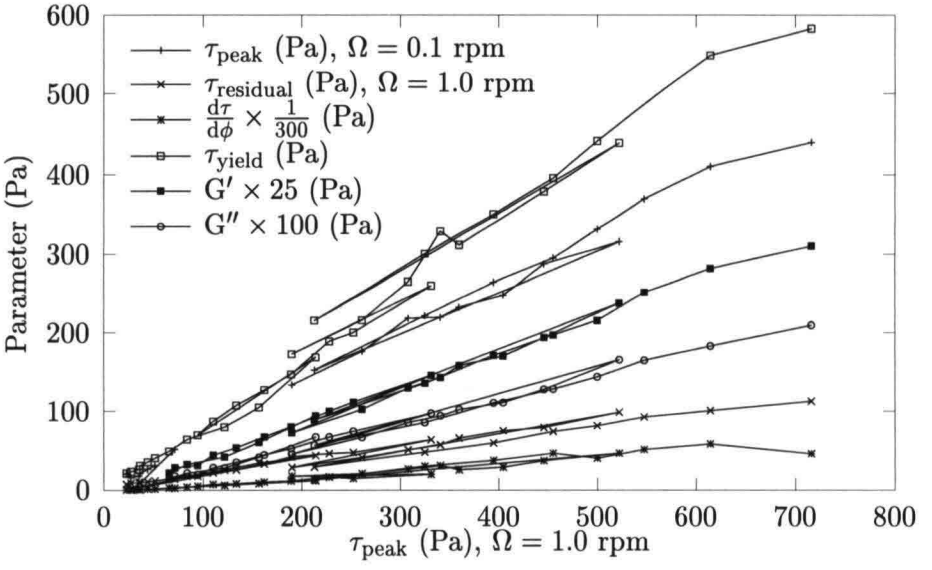

Figure 4.2: Dependencies between rheological strength parameters

Chapter 5

Acknowledgement

This work was funded jointly by the Netherlands Technolgy Foundation (STW) and the Commission of the European Communities, Directorate General for Science, Research and Development, under contract No MAS3-CT97-0082 (COSINUS-project). It was carried out in the framework of the Netherlands Centre for Coastal Research (NCK).

References

BEEN, K. 1980. *Stress–strain behaviour of a cohesive soil deposited under water.* Ph.D. thesis, Oxford University.

BERLAMONT, J., & VAN GOETHEM, J. 1984. *K.U.Leuven, Hydraulics Laboratory report to S.B.B.M.* Tech. rept. IWONL project A1/4-15321-4000. K.U.Leuven.

BERLAMONT, J., OCKENDEN, M., TOORMAN, E., & WINTERTERP, J. 1992. The Characterisation of Cohesive Sediment Properties. *Coastal Eng. Special Issue - Draft (Last modification: July 7 1992).*

BOWDEN, R.K. 1988. *Compression behaviour and shear strength characteristics of a natural silty clay sedimented in the laboratory.* Ph.D. thesis, Oxford University.

DE WIT, P.J. 1995. *Liquefaction of Cohesive Sediments caused by Waves.* Ph.D. thesis, Delft University of Technology, the Netherlands.

MERCKELBACH, L.M. 1998. *Laboratory experiments on consolidation and strength evolution of mud layers.* Tech. rept. 1-98. Delft University of Technology.

VAN KESSEL, T. 1997. *Generation and transport of subaqueous fluid mud layers.* Ph.D. thesis, Delft University of Technology.

WEAST, R.C. 1973. *Handbook of chemistry and physics.* 54^{th} edn. CRC PRESS.

List of Symbols

A	cross sectional area	m^2
A	calibration constant	kg m^{-3} V^{-1}
A	calibration constant	Pa
B	calibration constant	kg m^{-3}
B	calibration constant	–
c	concentration	g/l
c_s	concentration of calibration sample	g/l
e	void ratio	–
G'	storage modulus	Pa
G''	loss modulus	Pa
I	electircal current	Amp
k_1	calibration constant	g l^{-1}
k_2	calibration constant	g l^{-1} V^{-1}
k	permeability	m s^{-1}
l	height of vane	m
l	distance between electrodes	m
p_e	excess pore water pressure	Pa
r	radius of vane	m
r	resistivity	Ω m
R	resistance	Ω
t	time	s
T	measured torque	mNm
v_s	velocity of the particles	m s^{-1}
V	voltage	volt
V_0	voltage measurement of clear water	volt
V_s	voltage measurement of sample	volt
z	vertical ordinate	m

$\dot{\gamma}$	shear rate	s^{-1}
δ	loss angle	rad
η	dynamic differential viscosity	Pa s
ρ	density	kg m^{-3}
ρ_b	bulk density of the mud	kg m^{-3}
ρ_f	density of the pore water	kg m^{-3}
ρ_s	density of the solids	kg m^{-3}
σ'	effective stress	Pa
τ	shear stress	Pa
$\hat{\tau}$	amplitude of shear stress	Pa
τ_{peak}	peak shear stress	Pa
$\tau_{residual}$	residual shear stress	Pa
τ_{yield}	yield stress	Pa
ϕ	rotation angle	rad
$\hat{\phi}$	amplitude of rotation angle	rad
ϕ_{peak}	peak rotation angle	rad
ϕ_{yiels}	yield rotation angle	rad
ϕ_p	volume fraction of solids	–
ω	angular frequency	rad/s
Ω	angular velocity	rad/s

Appendix A

Figures

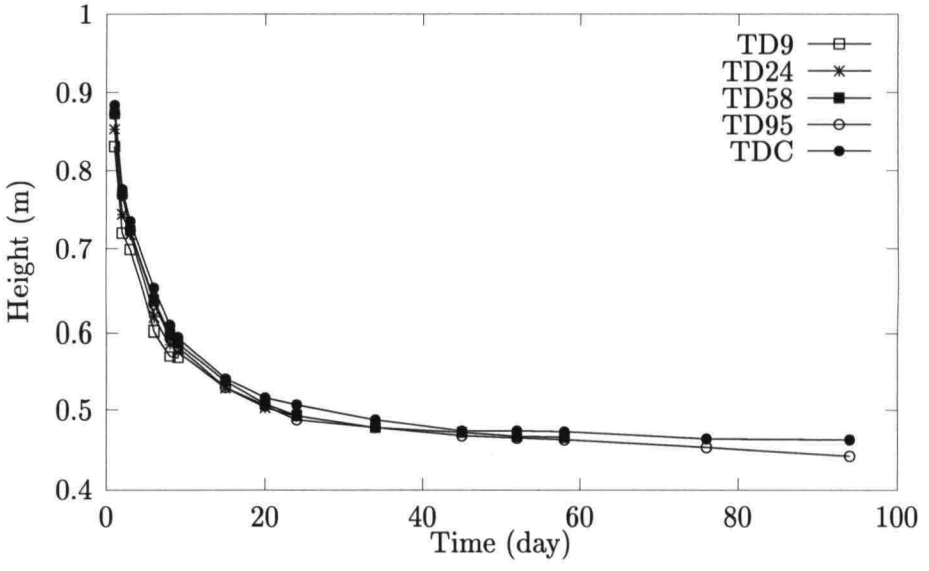

Figure A.1: Interface height with time

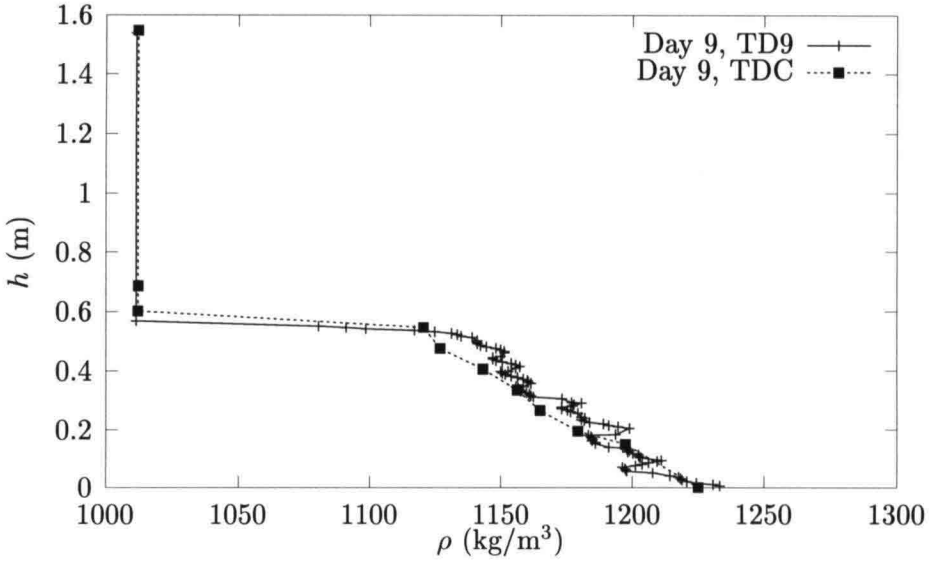

Figure A.2: Density profiles TD9

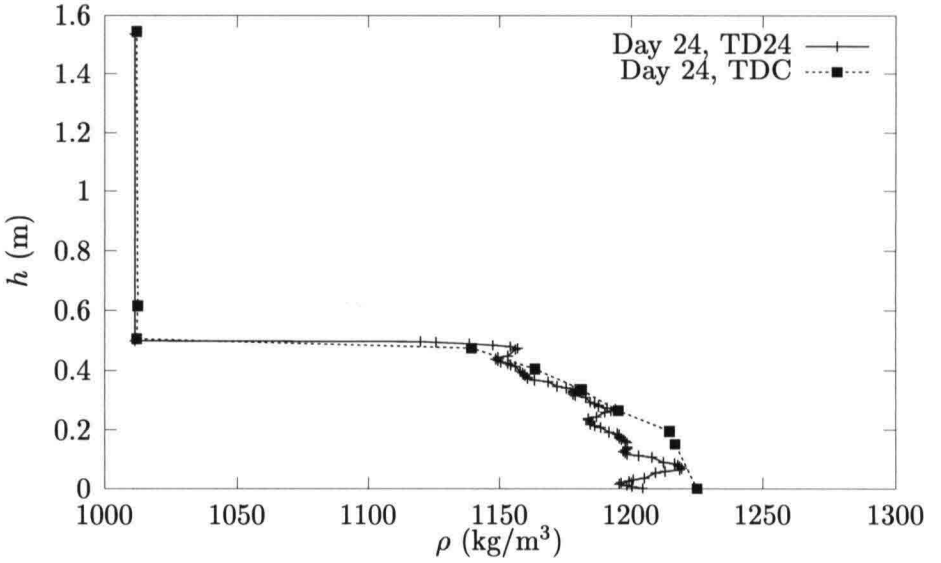

Figure A.3: Density profiles TD24

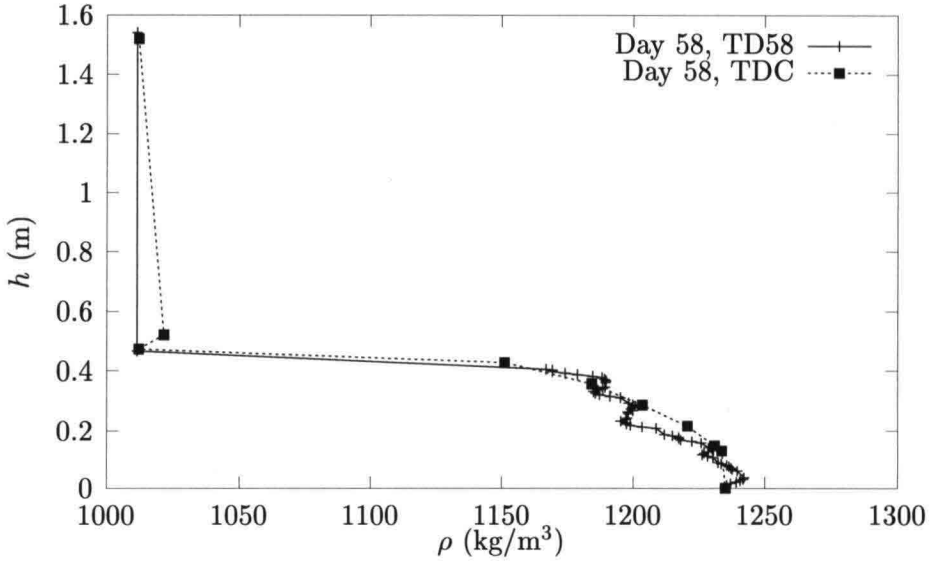

Figure A.4: Density profiles TD58

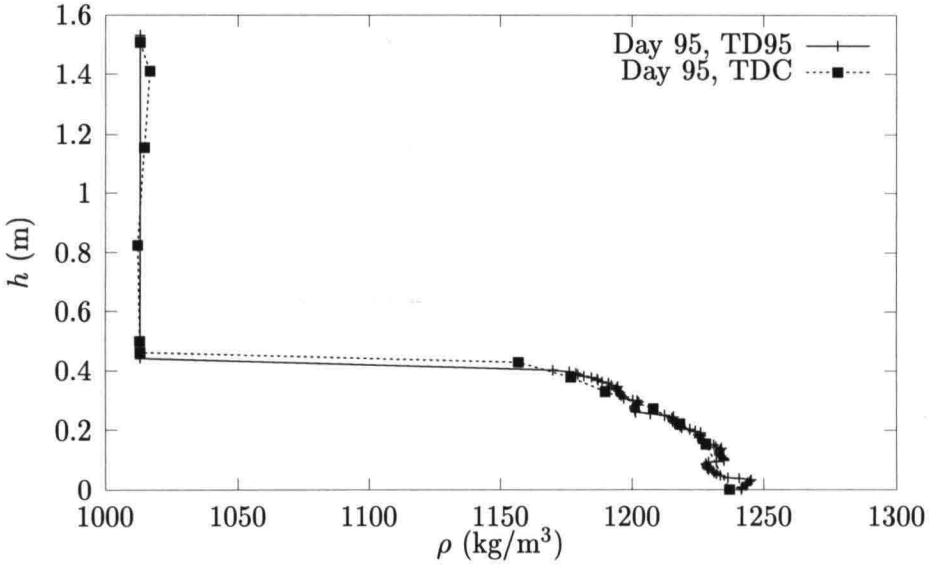

Figure A.5: Density profiles TD95

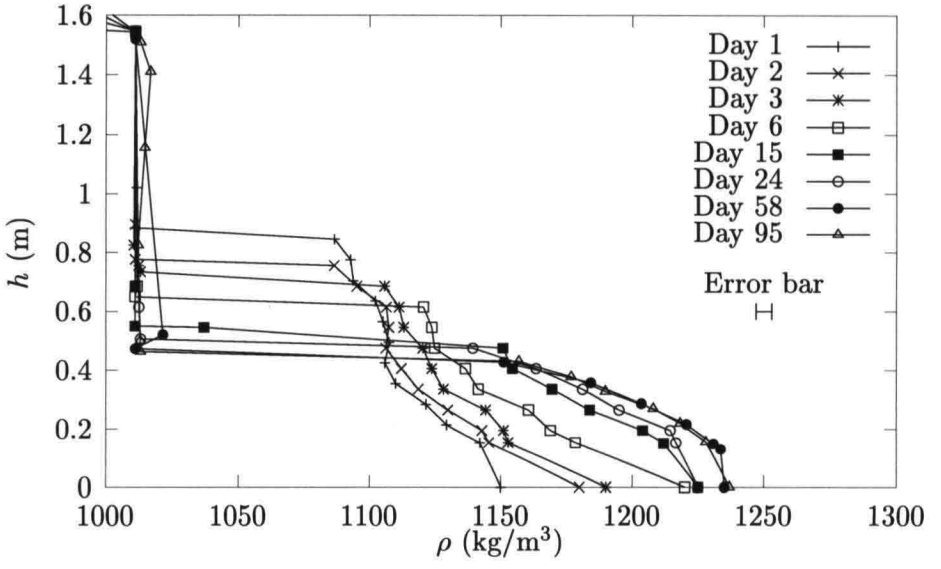

Figure A.6: Density profiles TDC

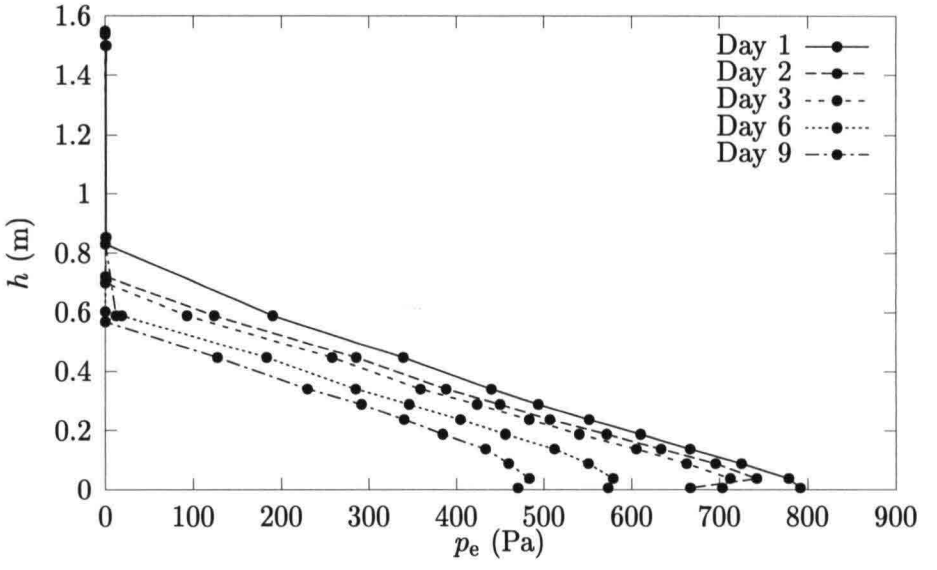

Figure A.7: Excess pore water pressure profiles TD9

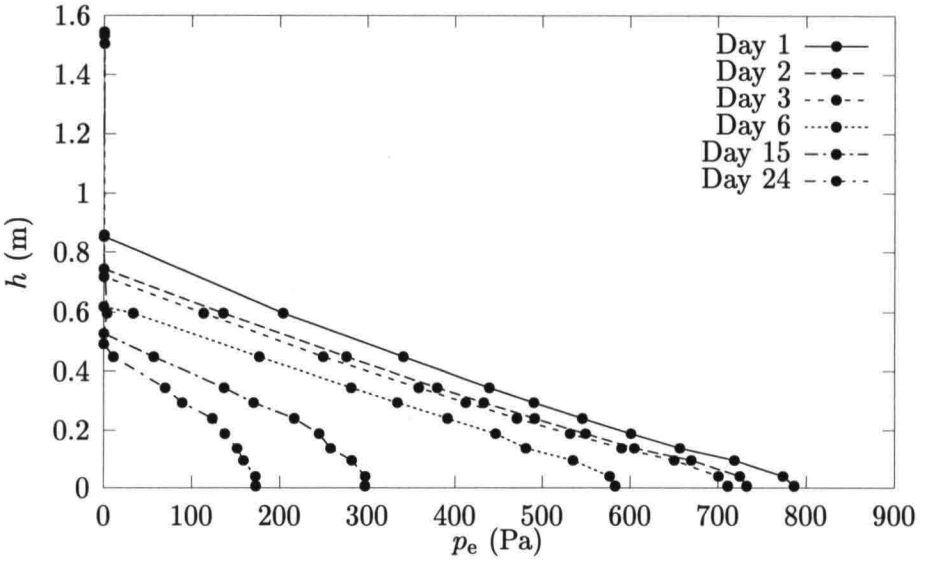

Figure A.8: Excess pore water pressure profiles TD24

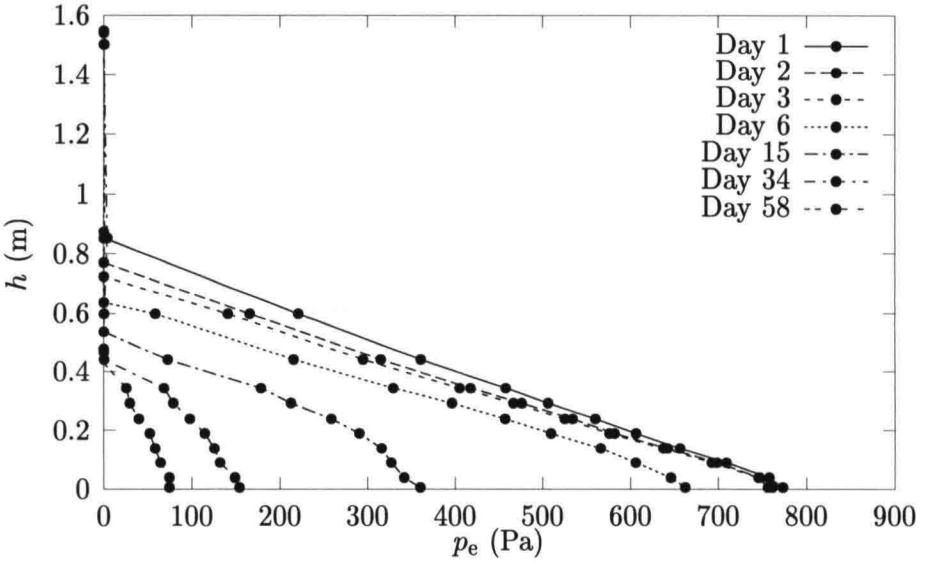

Figure A.9: Excess pore water pressure profiles TD58

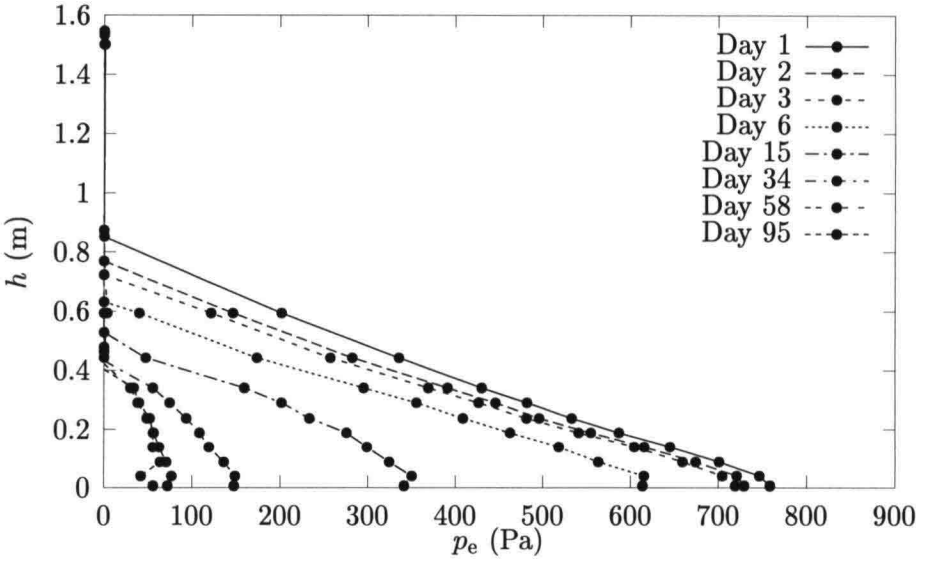

Figure A.10: Excess pore water pressure profiles TD95

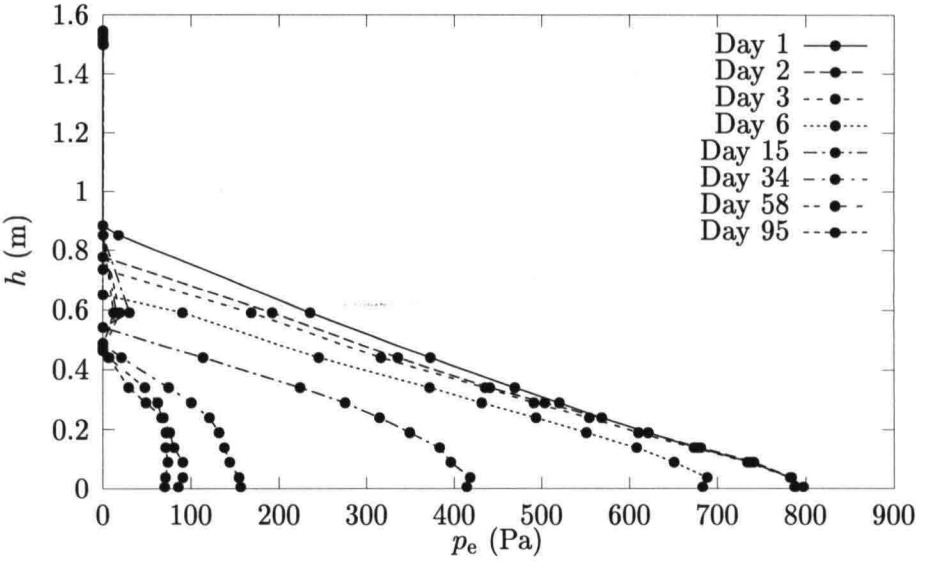

Figure A.11: Excess pore water pressure profiles TDC

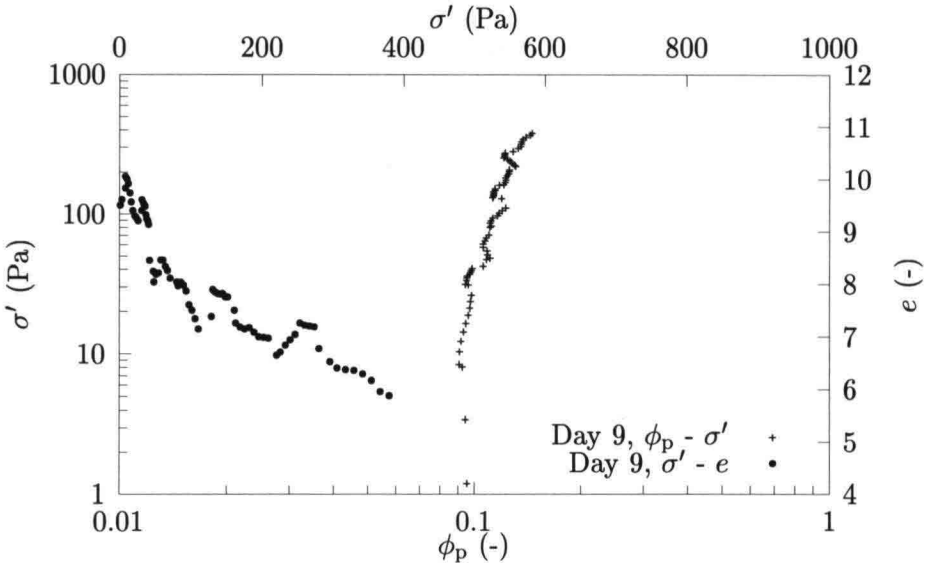

Figure A.12: Effective stresses at day 9, TD9

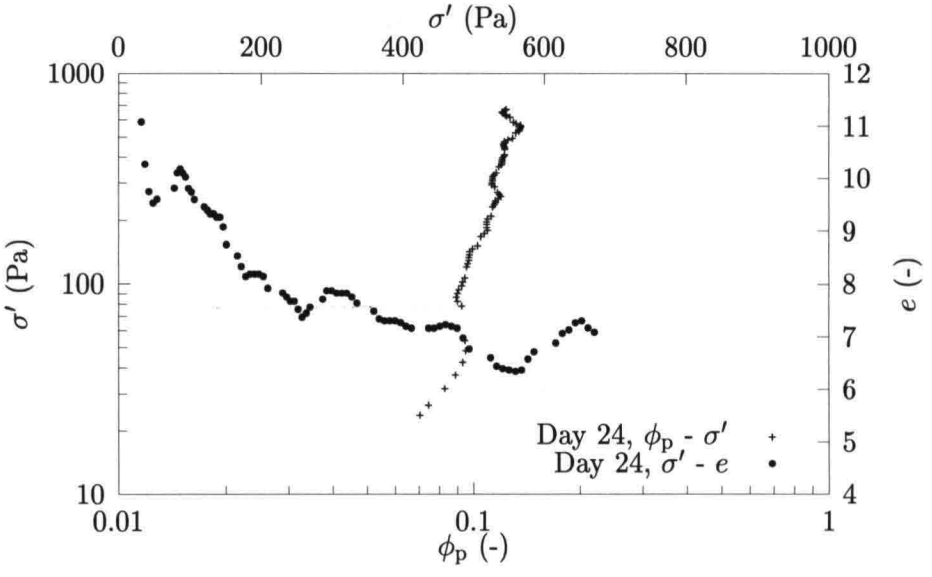

Figure A.13: Effective stresses at day 24, TD24

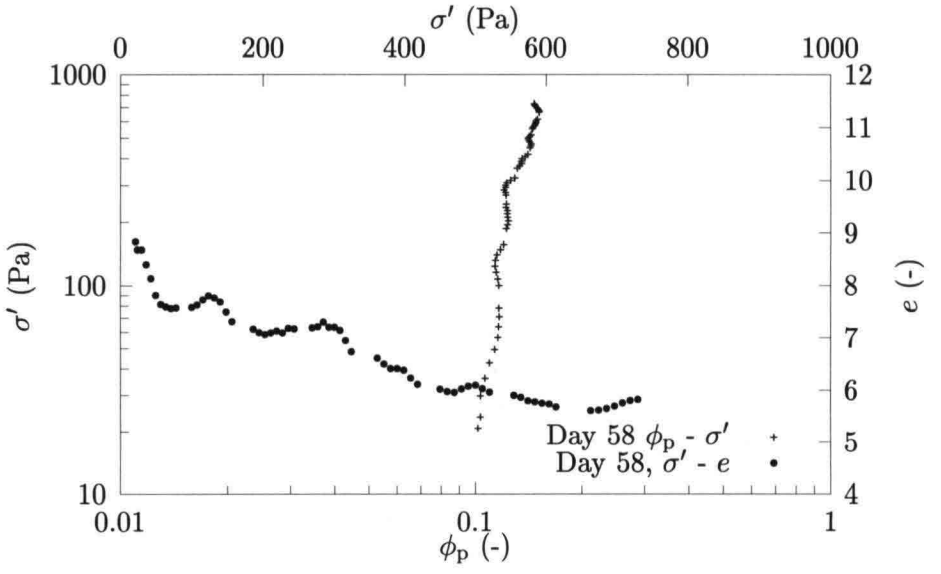

Figure A.14: Effective stresses at day 58, TD58

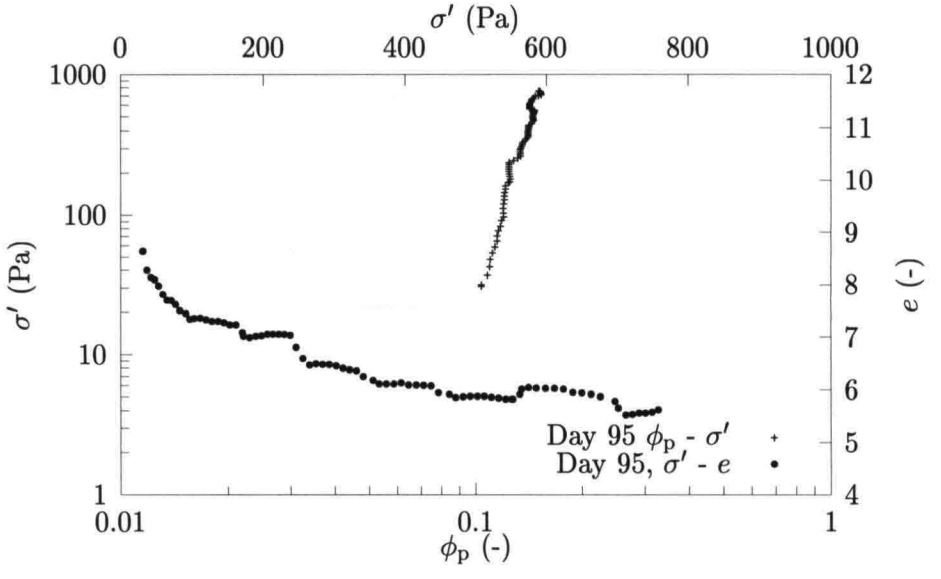

Figure A.15: Effective stresses at day 95, TD95

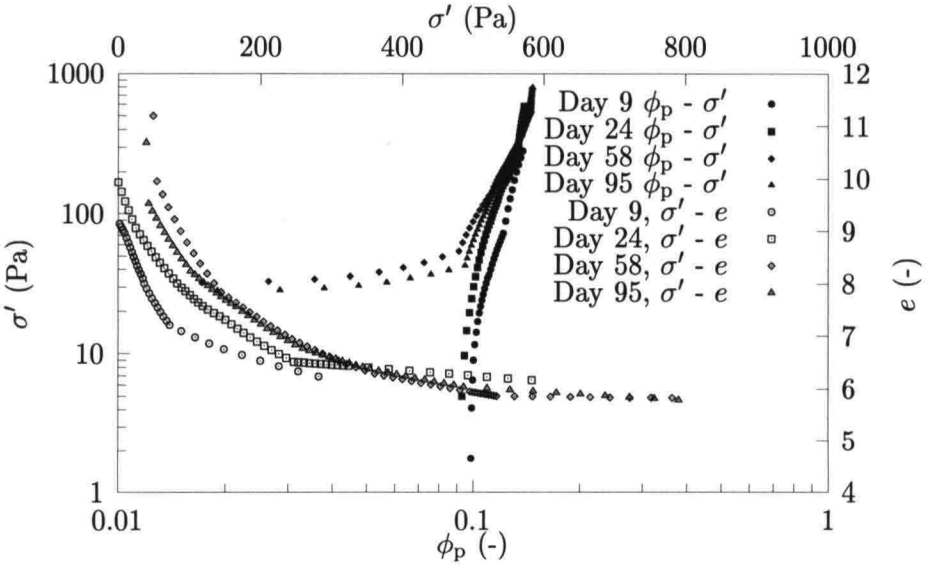

Figure A.16: Effective stresses TDC

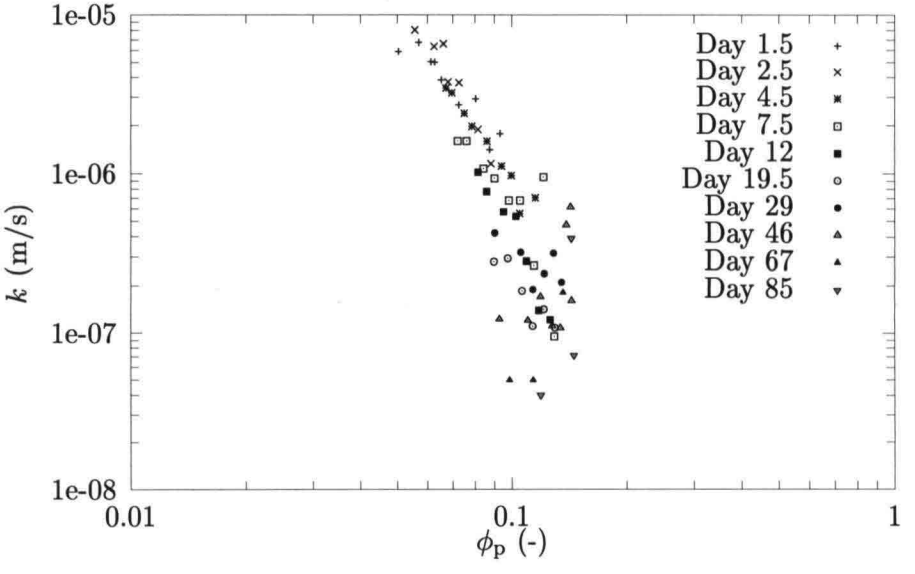

Figure A.17: Permeability data

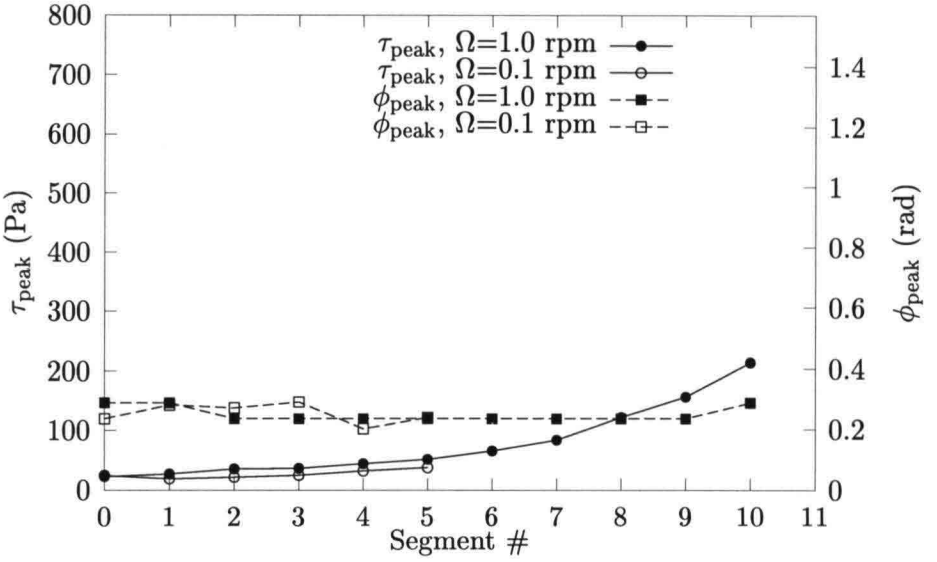

Figure A.18: Peak shear stresses and peak angles, TD9

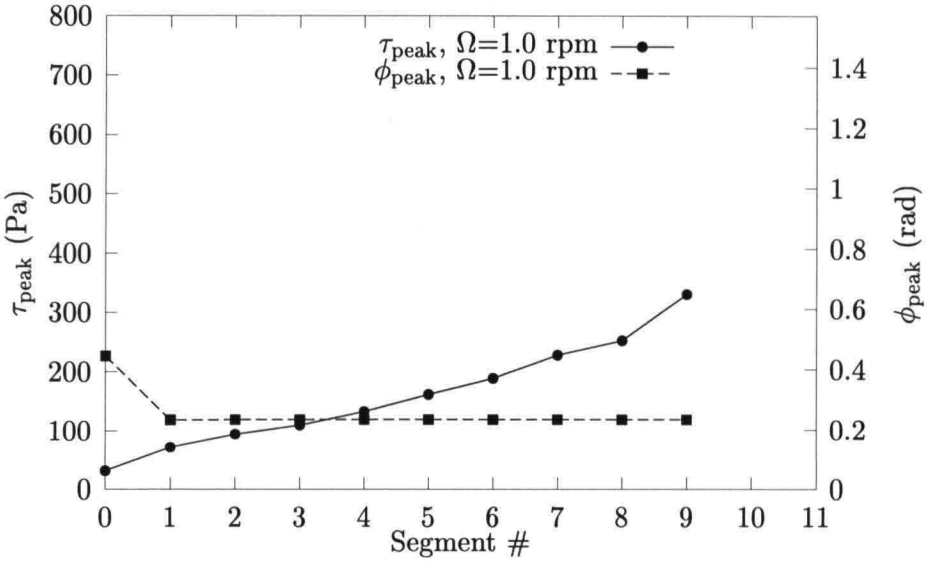

Figure A.19: Peak shear stresses and peak angles, TD24

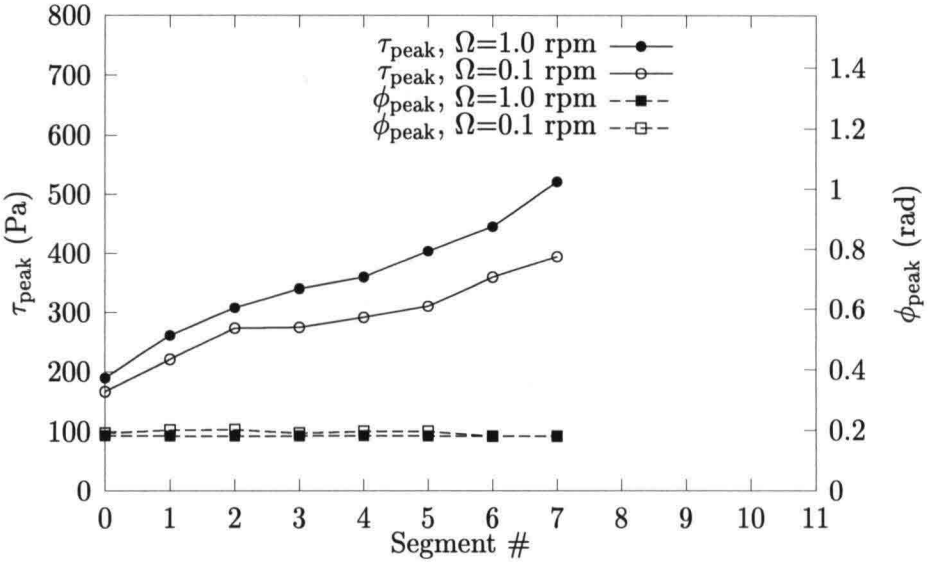

Figure A.20: Peak shear stresses and peak angles, TD58

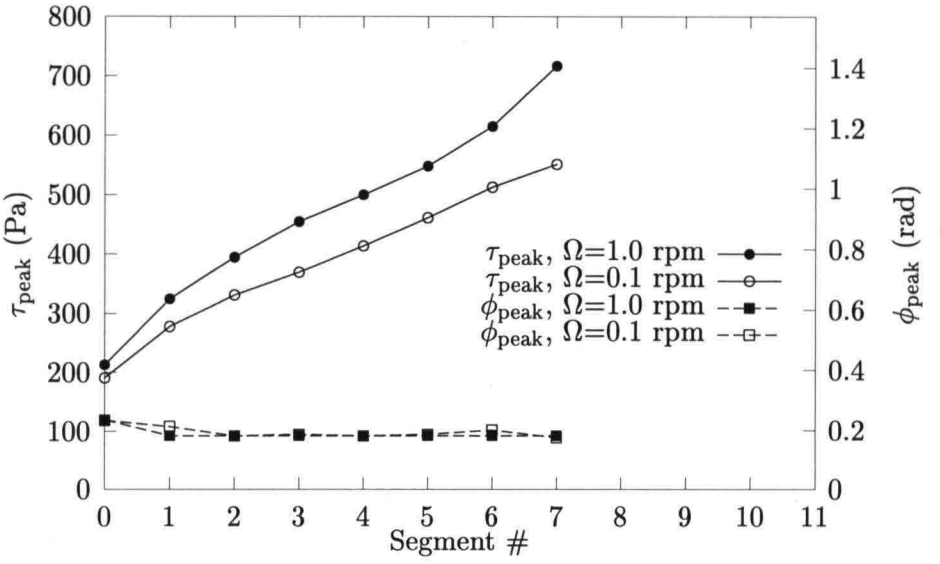

Figure A.21: Peak shear stresses and peak angles, TD95

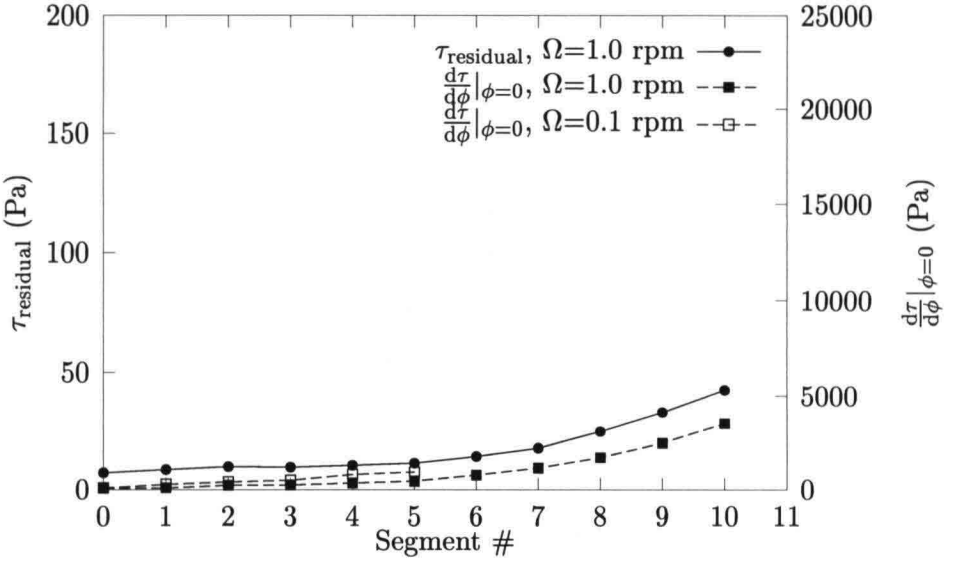

Figure A.22: Residual shear stresses and $\frac{d\tau}{d\phi}|_{\phi=0}$, TD9

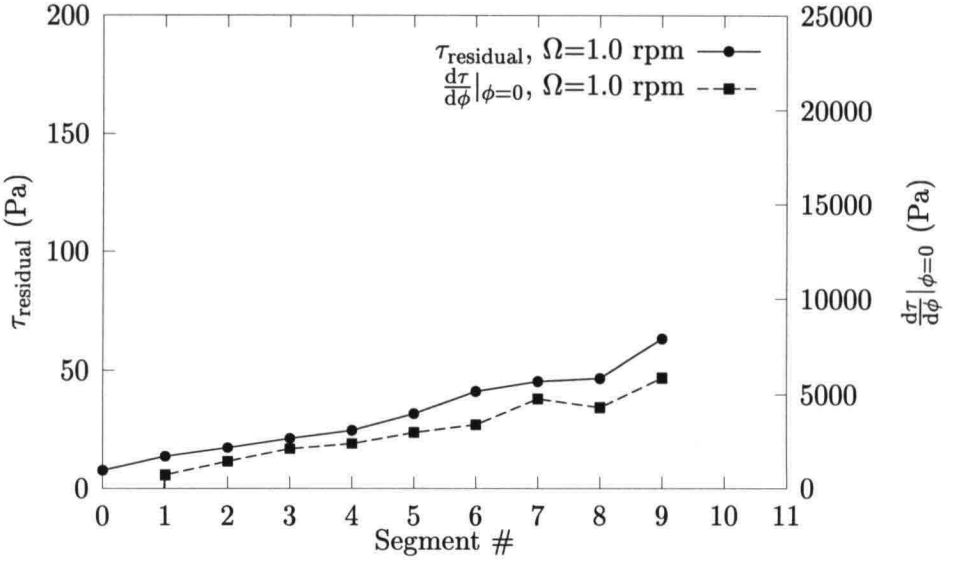

Figure A.23: Residual shear stresses and $\frac{d\tau}{d\phi}|_{\phi=0}$, TD24

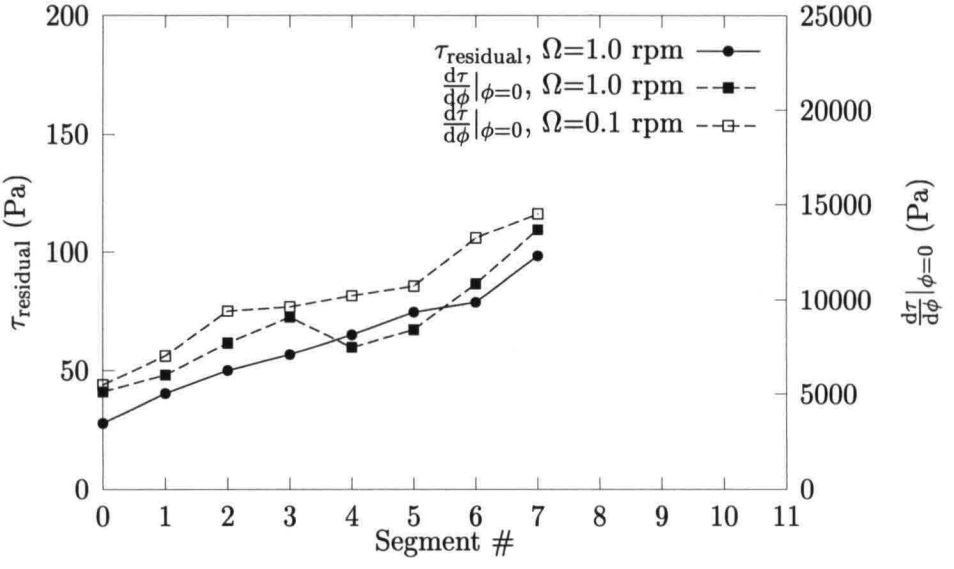

Figure A.24: Residual shear stresses and $\frac{d\tau}{d\phi}|_{\phi=0}$, TD58

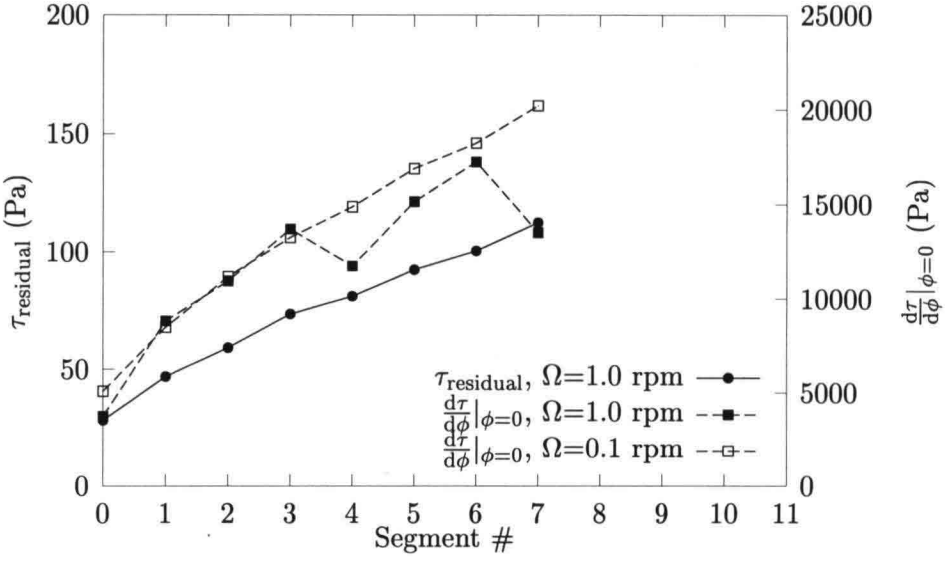

Figure A.25: Residual shear stresses and $\frac{d\tau}{d\phi}|_{\phi=0}$, TD95

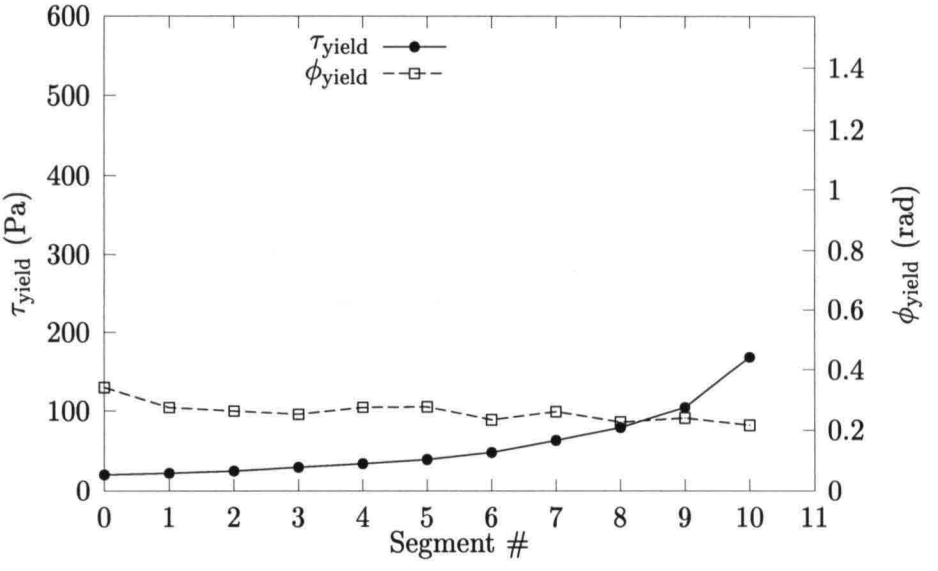

Figure A.26: Yield stresses and yield angles, TD9

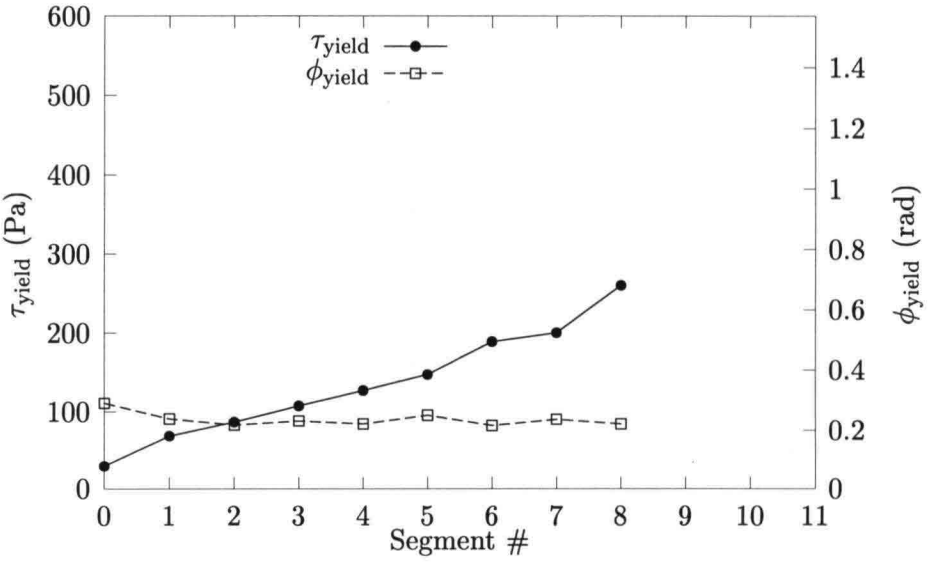

Figure A.27: Yield stresses and yield angles, TD24

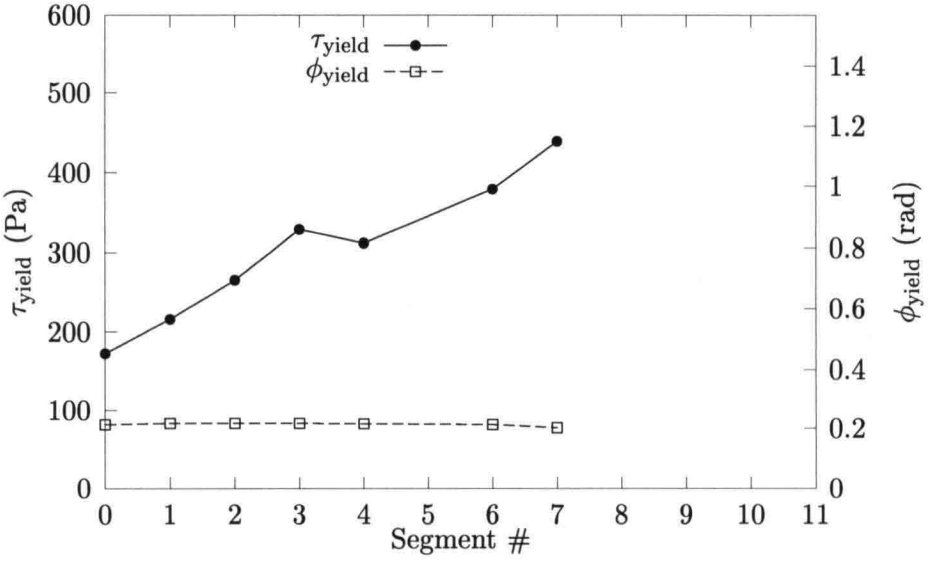

Figure A.28: Yield stresses and yield angles, TD58

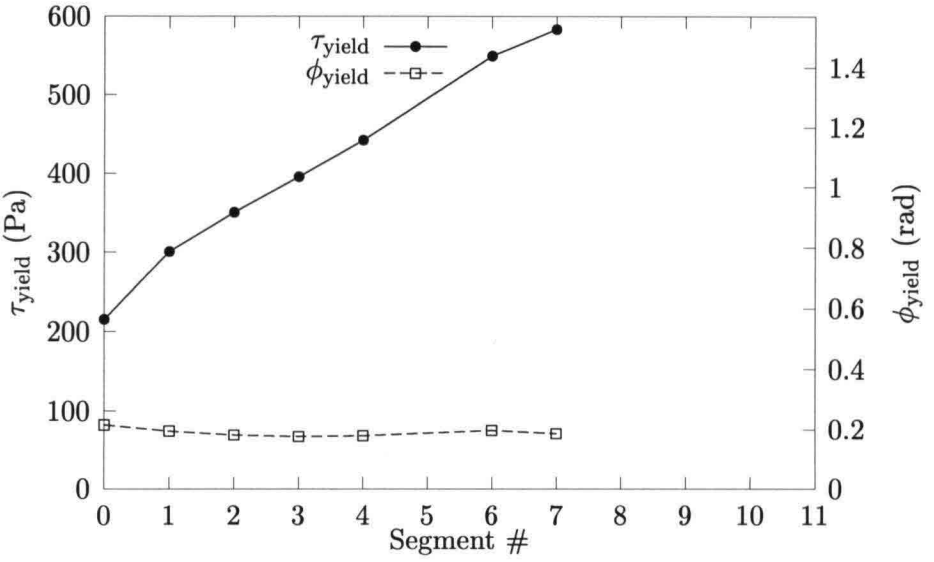

Figure A.29: Yield stresses and yield angles, TD95

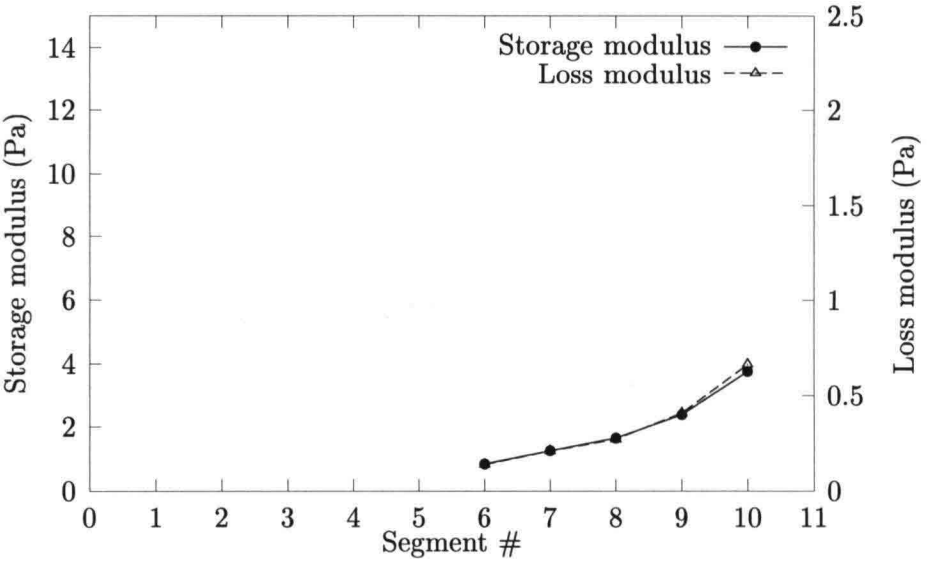

Figure A.30: Storage and loss moduli for $\omega = 1.57$ rad/s, TD9

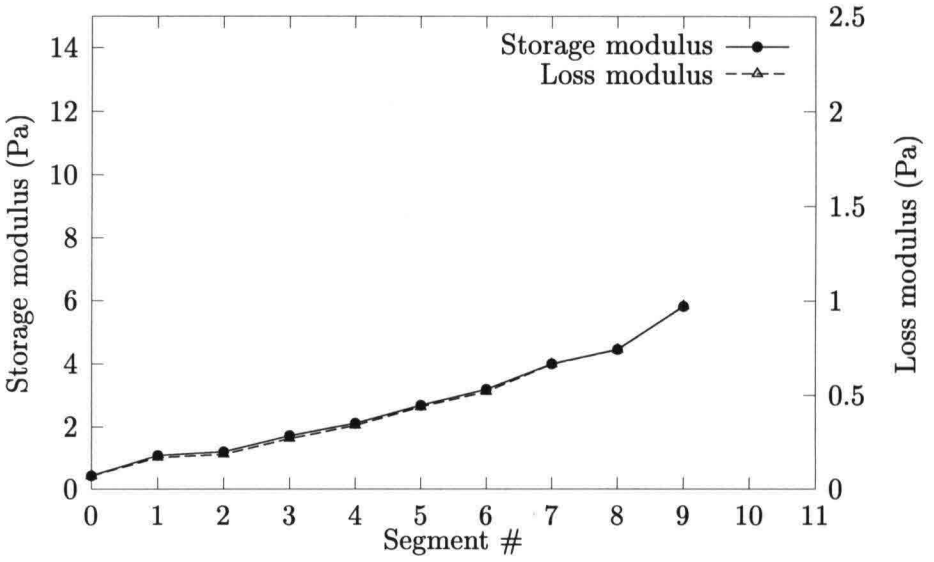

Figure A.31: Storage and loss moduli for $\omega = 1.57$ rad/s, TD24

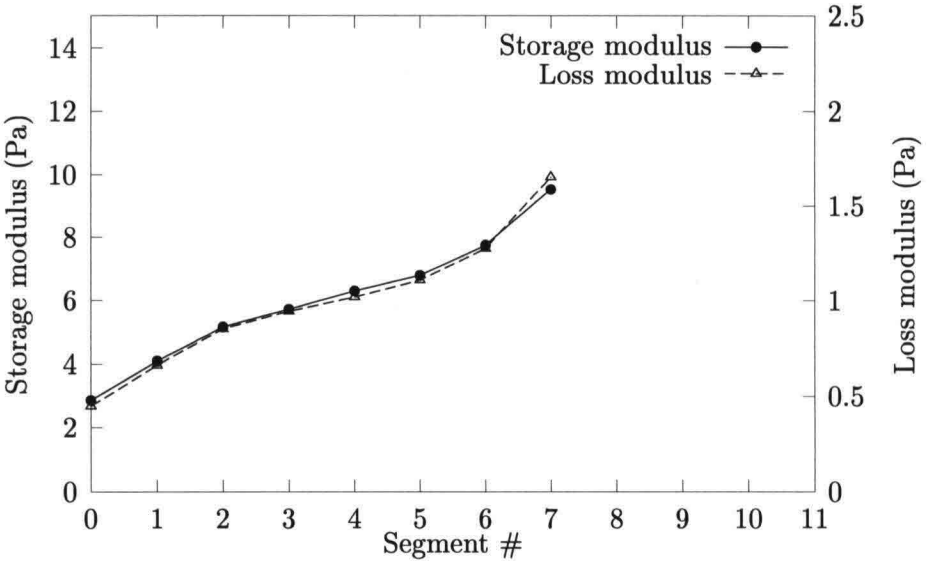

Figure A.32: Storage and loss moduli for $\omega = 1.57$ rad/s, TD58

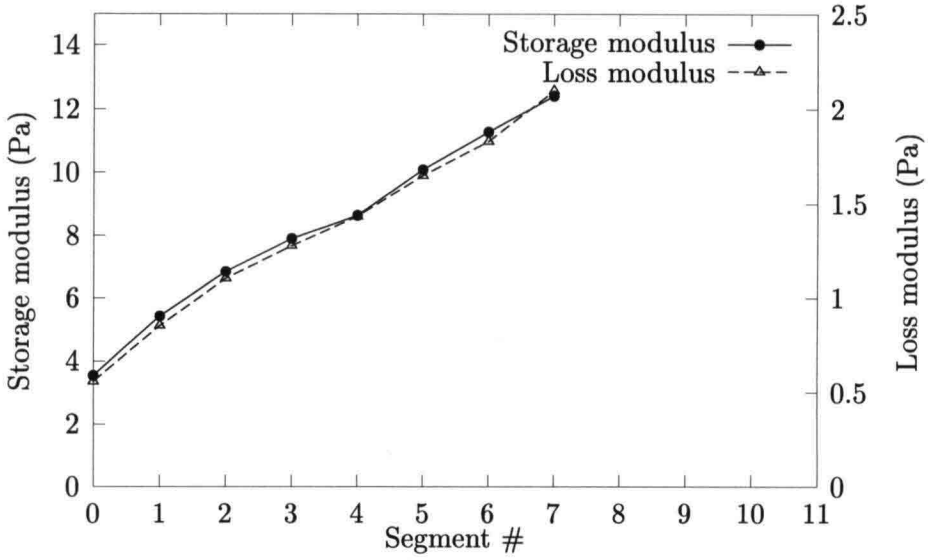

Figure A.33: Storage and loss moduli for $\omega = 1.57$ rad/s, TD95

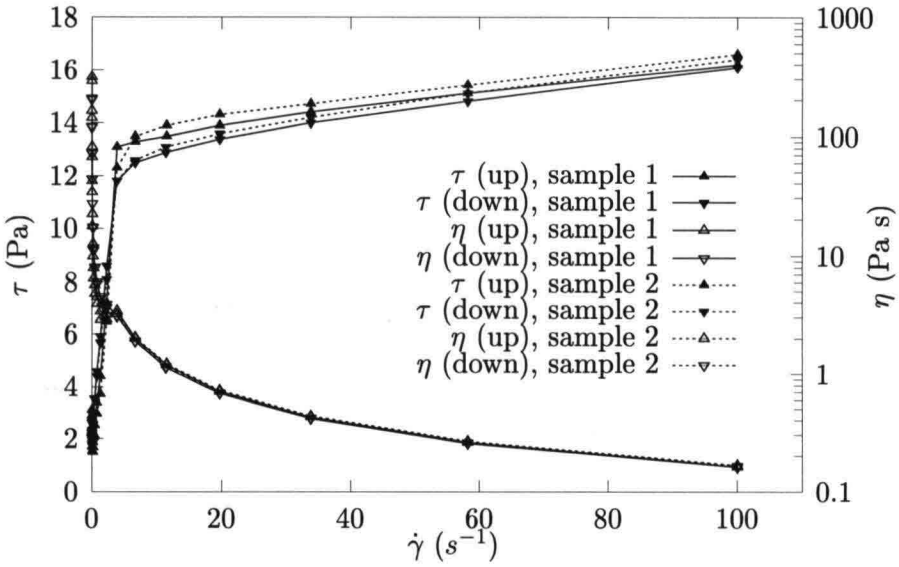

Figure A.34: Flow curves and dynamic viscosities, TDC

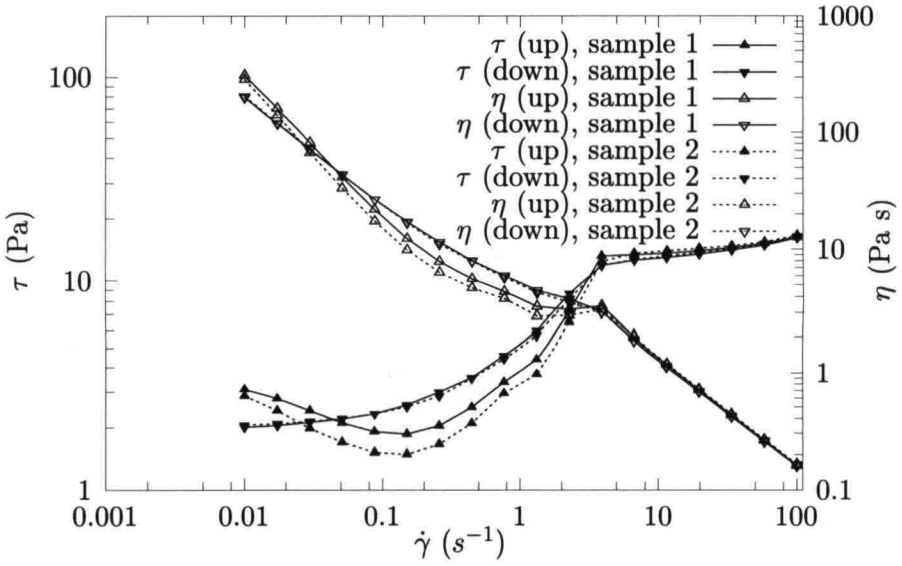

Figure A.35: Flow curves and dynamic viscosities, TDC